HHS Public Access

Author manuscript

J Physiol. Author manuscript; available in PMC 2022 July 26.

Published in final edited form as:

J Physiol. 2021 June ; 599(12): 3195–3220. doi:10.1113/JP281544.

Rapid volume pulsation of the extracellular space coincides with epileptiform activity in mice and depends on the NBCe1 transporter

Robert Colbourn[1,2], **Jan Hrabe**[1,3], **Charles Nicholson**[1,4], **Matthew Perkins**[1], **Jeffrey H. Goodman**[5,6,7,8], **Sabina Hrabetova**[1,8]

[1]Department of Cell Biology, SUNY Downstate Health Sciences University, Brooklyn, New York, USA

[2]Neural and Behavioral Science Graduate Program, SUNY Downstate Health Sciences University, Brooklyn, New York, USA

[3]Medical Physics Laboratory, Center for Biomedical Imaging and Neuromodulation, Nathan S. Kline Institute, Orangeburg, New York, USA

[4]Department of Neuroscience and Physiology, NYU Grossman School of Medicine, New York, New York, USA

[5]Department of Developmental Neurobiology, The New York State Institute for Basic Research in Developmental Disabilities, Staten Island, New York, USA

[6]Department of Physiology and Pharmacology, SUNY Downstate Health Sciences University, Brooklyn, New York, USA

[7]Department of Neurology, SUNY Downstate Health Sciences University, Brooklyn, New York, USA

[8]The Robert F. Furchgott Center for Neural and Behavioral Science, SUNY Downstate Health Sciences University, Brooklyn, New York, USA

Abstract

The extracellular space (ECS) of the brain shrinks persistently by approximately 35% during epileptic seizures. Here we report the discovery of rapid volume pulsation (RVP), further transient

Corresponding author S. Hrabetova: Department of Cell Biology, SUNY Downstate Health Sciences University, 450 Clarkson Avenue, MSC 5, Brooklyn, New York 11203, USA. sabina.hrabetova@downstate.edu.

Author contributions

Research was performed at SUNY Downstate Health Sciences University. R.C. and S.H. conceived the project. R.C., J.G. and S.H. designed the experiments. R.C., J.H., M.P. and S.H. acquired and analysed data. R.C. and C.N. wrote the Octave and MATLAB software used for the data analysis. R.C., J.H., C.N., J.G. and S.H. interpreted the data. The manuscript was drafted by R.C. and edited by R.C., J.H., C.N., M.P., J.G. and S.H. All authors approved the final version of the manuscript and they will ensure that questions related to the accuracy or integrity of any part of their work are appropriately investigated and resolved. All persons designated as authors qualify for authorship, and all those who qualify for authorship are listed.

Competing interests

The authors have no competing interests to declare.

Supporting information

Additional supporting information may be found online in the Supporting Information section at the end of the article.

Statistical Summary Document

Data set of RVP and LFP induced by 4-AP

drops in ECS volume which accompany events of epileptiform activity. These transient ECS contractions were observed in multiple mouse models of epileptiform activity both *in vivo* (bicuculline methiodide model) and *in vitro* (hyaluronan synthase 3 knock-out, picrotoxin, bicuculline and 4-aminopyridine models). By using the probe transients quantification (PTQ) method we show that individual pulses of RVP shrank the ECS by almost 15% *in vivo*. In the 4-aminopyridine *in vitro* model, the individual pulses of RVP shrank the ECS by more than 4%, and these transient changes were superimposed on a persistent ECS shrinkage of 36% measured with the real-time iontophoretic method. In this *in vitro* model, we investigated several channels and transporters that may be required for the generation of RVP and epileptiform activity. Pharmacological blockages of $Na^+/K^+/2Cl^-$ cotransporter type 1 (NKCC1), K^+/Cl^- cotransporter (KCC2), the water channel aquaporin-4 (AQP4) and inwardly rectifying potassium channel 4.1 (Kir4.1) were ineffective in halting the RVP and the epileptiform activity. In contrast, pharmacological blockade of the electrogenic Na^+/HCO_3^- cotransporter (NBCe1) by 4,4'-diisothiocyano-2,2'-stilbenedisulfonic acid (DIDS) eliminated both the RVP and the persistent ECS shrinkage. Importantly, this blocker also stopped the epileptiform activity. These results demonstrate that RVP is closely associated with epileptiform activity across several models of epileptiform activity and therefore the underlying mechanism could potentially represent a novel target for epilepsy management and treatment.

Keywords

4,4'-diisothiocyano-2,2'-stilbenedisulfonic acid (DIDS); 4-aminopyridine (4-AP); epileptiform activity; extracellular space (ECS); Na^+/HCO_3^- cotransporter (NBCe1); probe transients quantification (PTQ) method; rapid volume pulsation (RVP); tetramethylammonium (TMA)

Introduction

The generation of seizure activity requires a population of local neuronal circuits to exist in a pathologically hyperexcitable and synchronous state. Understanding how neuronal circuits come into such states should provide an avenue to new treatments for seizures and epilepsy. The need for this is evident because approximately 30% of all epilepsies resist pharmaceutical interventions (Dalic & Cook, 2016). Current treatments often target neuronal firing (Goldenberg, 2010). Not frequently considered at this time is the role of the extracellular space (ECS), even though it is known that the ECS shrinks by about 35% of its normal size for the duration of the epileptiform activity (Lux *et al.* 1986; Slais *et al.* 2008; Tønnesen *et al.* 2018); here we call this persisting reduction in ECS a 'slow ECS shrinkage' (SES). It is also known that ECS shrinkage facilitates the generation of hyperexcitability and synchrony by increasing the extracellular concentration of neuroactive substances (Andrew & MacVicar, 1994; Kilb *et al.* 2006) and by enhancing ephaptic interactions between depolarizing cells (Dudek *et al.* 1986; Weiss & Faber, 2010).

We discovered a new type of reduction in ECS volume during epileptiform activity, namely a 'rapid volume pulsation' (RVP). Such RVP has not been reported before, presumably because techniques were not fast enough to record it. RVP typically consists of many chained individual events. During each RVP event, the ECS shrinks rapidly, then expands

more slowly back to baseline volume in the same time frame as each event of the epileptiform activity. It is possible that the molecular mechanism that generates RVP resembles that underlying SES. Dietzel *et al.* (1989) thought that SES was a consequence of increased neuronal firing and the resultant transmembrane fluxes of ions, namely Na^+, K^+ and Cl^-. The result of these currents is a net decrease of ionic concentration in the ECS causing water to shift from the ECS into cells, thus swelling the cells and shrinking the ECS (Dietzel *et al.* 1980). Transporters and channels that are involved in the transmembrane movement of these ions could therefore be involved in the generation of both SES and RVP during epileptiform activity and seizures. In addition to those, we also investigated transporters that do not rely on osmotic forces and that have been studied in connection with a neuronal activity-induced transient shrinkage of ECS (for a review, see MacAulay, 2020). RVP may share the mechanisms of activity-induced shrinkage of the ECS because both phenomena accompany neuronal depolarization.

We focused on five transporters and channels as potential players in the generation of RVP. The neuronal $Na^+/K^+/2Cl^-$ cotransporter type 1 (NKCC1) and K^+/Cl^- cotransporter (KCC2) were chosen because of their involvement in Na^+, K^+ and Cl^- regulation and because the blockers of these channels, furosemide and bumetanide, impede epileptiform activity in some models (Hochman, 2012; Uwera *et al.* 2015, Liu *et al.* 2020). We also looked at several channels and transporters present on astrocytes because astrocytes are thought to swell during neuronal hyperexcitability (Dietzel *et al.* 1989; Murphy *et al.* 2017*a*) and thereby cause SES. We investigated the water channel aquaporin-4 (AQP4) because previous AQP4-KO studies showed a higher seizure threshold and increased seizure duration in these animals (Binder *et al.* 2006), as well as increased cerebral oedema (Lee *et al.* 2012). The inwardly rectifying potassium channel 4.1 (Kir4.1), a dominant mediator of astrocytic K^+ conductance, was selected because both its function and its expression change in epilepsy (Ohno *et al.* 2015; Nwaobi *et al.* 2016). Finally, the electrogenic Na^+/HCO_3^- cotransporter (NBCe1) was investigated because it is involved in activity-induced shrinkage of the ECS (Larsen & MacAulay, 2017).

Our study had four goals: (1) to establish whether RVP commonly occurred across multiple models of epileptiform activity, (2) to quantify RVP in established *in vitro* and *in vivo* models of epileptiform activity, (3) to identify transporter and channel blockers that diminish both the RVP and the epileptiform activity, and (4) to determine whether a blocker that diminishes RVP and epileptiform activity inhibits SES as well.

To identify and quantify RVP, we used the fast-responding probe transients quantification (PTQ) technique. For goal 1, we used a diverse set of mouse models of epileptiform activity and established that RVP generation is not dependent on a particular epileptogenic mechanism. For goal 2, we looked at two pharmacological models of epileptiform activity —4-aminopyridine (4-AP) (Gonzalez-Sulser *et al.* 2011) set up *in vitro* and bicuculline methiodide (Xiong *et al.* 2017) set up *in vivo*—and determined that RVP always accompanies epileptiform events in both. We also quantified RVP events in terms of their frequency and amplitude. To accomplish goal 3, we used the 4-AP *in vitro* model to quantify RVP, then applied pharmacological agents that block the transporters or channels listed above to see if they reduce the magnitude of RVP and mitigate epileptiform activity. We

found that NBCe1 blockade inhibited both RVP and epileptiform activity. To accomplish goal 4, the real-time iontophoretic (RTI) technique (Nicholson & Phillips, 1981; Odackal *et al.* 2017) was used to quantify the SES in the 4-AP model and show that NBCe1 blockade reverses the SES.

Methods

Ethical approval

All experiments were performed at SUNY Downstate Health Sciences University in accordance with all NIH and local IACUC regulations. The investigators all understand the *Journal of Physiology*'s ethical principles and all work complied with their animal ethics checklist. Hyaluronan synthase 3 knock-out (Has3KO) mice were obtained from Dr Yu Yamaguchi (Sanford Children's Health Research Center, SanfordBurnham Prebys Medical Discovery Institute, La Jolla, California) and were of C57BL/6 background. All other experiments used wild-type C57BL/6 mice that were purchased from Charles River Laboratories. The SUNY Downstate Health Sciences University core animal facility housed all the mice in a 12 h light–dark cycle and provided continuous access to food and drinking water. Mice weighed 18–42 g and were between 7 weeks and 6 months of age. The ECS parameters are known to be consistent during this period (Syková & Nicholson, 2008). All experimental groups contained both male and female mice because control ECS parameters are similar between the two sexes in this age group (Syková *et al.* 2005). For *in vitro* experiments, several different anaesthetics were used prior to decapitation and brain slice preparation. Sodium pentobarbital (50 mg/kg injected I.P.) (cat #P3761, Sigma-Aldrich; St. Louis, MO, USA) was administered to the Has3KO animals. Animals for phase 1 PTQ experiments were anaesthetized using inhaled halothane (cat #B4388; Sigma-Aldrich). Animals for phase 2 PTQ experiments and RTI experiments were anaesthetized with urethane (1.8 g/kg injected I.P.) (cat #U2500, Sigma-Aldrich).

For *in vivo* recordings, urethane (1.8 g/kg injected I.P.) (cat #U2500, Sigma-Aldrich) was administered to the mice to induce anaesthesia, and the mice were given a 10% boost of urethane as needed if depth of anaesthesia was deemed insufficient. In addition, small boluses of lidocaine (2%) (cat #L-2000–05, Covetrus; Dublin, OH, USA) were locally administered in the skin overlying the skull to provide local analgesia. *N* counts only include mice that had stable vital signs for the duration of the experiment. After data collection, the animals were killed by decapitation while still anaesthetized with urethane.

Artificial cerebrospinal fluid (ACSF) solutions

Table 1 lists the compositions of all ACSF solutions used, their purposes and how they are referred to in this manuscript. All experiments started with a control ACSF that was gassed continuously with a 95% O_2 and 5% CO_2 mixture to buffer at pH 7.4. All *in vitro* PTQ and RTI experiments also required the addition of 0.5 mM of an ECS molecular probe: tetramethylammonium-chloride (TMA-Cl) for all experiments except for experiments where α-naphthalene sulfonate was used. All *in vivo* PTQ experiments used control ACSF to bathe the brain surface, except that the concentration of TMA-Cl was increased to 1.0 mM. Table 1 also lists the different ACSFs that induced epileptiform activity (chemoconvulsant ACSFs)

and the ACSFs that blocked specific cellular transporters and channels (blocker ACSFs). A freezing point-depression osmometer (Osmette A No.5002; Precision Systems, Natick, MA, USA) measured the osmolarities of ACSF solutions to ensure they were between 295 and 305 mOsm (Sherpa *et al.* 2014).

In vitro brain slice preparation

Coronal slices 400 μm thick containing hippocampus or visual cortex were prepared using a vibratome (Leica VT1000 S; Leica Microsystems GmbH, Wetzlar, Germany) while the brain was immersed in pre-cooled control ACSF (Table 1). Brain slices recovered at room temperature in control ACSF that was gassed continuously with the 95% O_2 and 5% CO_2 mixture.

In vivo brain preparation

Mice were anaesthetized and placed in a head holder (model SG-4 N, Narishige Scientific Instrument Lab, Tokyo, Japan). A warming pad and rectal temperature probe kept the animal's core temperature stable, and pulse oximetry and heart rate readings were taken to monitor the animal's health during the procedure (Physiosuite; Kent Scientific Corporation, Torrington, CT, USA). A craniotomy exposed the visual cortex of a single hemisphere of the brain, and the dura was removed. After craniotomy, the anaesthetized mouse had a well, fabricated from a plastic ring, adhered to the surface of the skull and the surrounding skin with dental cement. ACSF flowed into and out of this well at a rate of 2.0 ml/min.

Ion-selective microelectrode (ISM) fabrication

Double-barrelled ISMs were fabricated according to a standard protocol (Odackal *et al.* 2017). All ISMs were made from double-barrelled theta glass (TG200–4; Warner Instruments Corp., Hamden, CT, USA). TMA-sensitive ISMs had the ion-sensitive barrel backfilled with 150 mM TMA-Cl in water, and the reference barrel filled with 150 mM NaCl. The tip of the ion-sensitive barrel was filled with a tetraphenylborate-based ion exchanger that detects TMA^+ (Corning exchanger 477317; currently available as IE 190 from WPI, Sarasota, FL, USA). The α-naphthalene sulfonate-sensitive ISMs (Nicholson & Phillips, 1981) were made similarly, except the ion-sensitive barrel was backfilled with 150 mM Na-naphthalene sulfonate and the tip was filled with an exchanger sensitive to α-naphthalene sulfonate made from 10 mM Crystal Violet (Cat # C0775, Sigma-Aldrich) dissolved in 3-nitro-o-xylene. All ISMs were calibrated in a set of five standard solutions before and after each experiment. The voltages were fitted to the Nicolsky equation to obtain the slope and interference values that are necessary for the conversion of voltages to concentrations. Experiments using ISMs with slope values that did not match before and after to within 10% were deemed unacceptable.

Electrophysiology recording setup

All of the *in vitro* experiments were performed with a common electrophysiology setup. Brain slices were placed in a submersion tissue chamber (Warner model RC-27L; Harvard Apparatus, Holliston, MA, USA) and superfused with ACSF at a flow rate of 2.0 ml/min. The temperature of the ACSF was kept at 34°C using a dual automatic temperature

controller (Warner model TC-344B; Harvard Apparatus) operating an in-line heater (Warner model SH-27A; Harvard Apparatus) along with a chamber heating system.

The *in vitro* recording setup was composed of a Gibraltar fixed-stage (07538-M-00; EXFO Photonic Solutions, Ontario, Canada) mounted with a compound microscope (BX51W1; Olympus America Inc., Melville, NY, USA) that had a CCD camera attached (OLY 150; Olympus America Inc.) to monitor microelectrode placement using infra-red illumination. In both *in vitro* PTQ and RTI experiments, the microelectrodes were positioned by robotic micromanipulators (MP285; Sutter Instruments Co., Novato, CA, USA). The ISM was connected to a dual-channel microelectrode amplifier (model IX2–700; Dagan Corp., Minneapolis, MN, USA) through two headstages (model 7100, $N = 0.001$ for ion-selective barrel, $N = 0.1$ for reference barrel; Dagan Corp), which provided a 10× gain to both the ion and reference barrel signals. The amplifier also continuously subtracted the reference from the ion signal. The subtracted ion signal and the reference signal were then routed to a Cyberamp 380 signal conditioner (Axon Instruments Inc., Union City, CA, USA), which provided an additional 10× gain and a 2 Hz low-pass 4-pole Bessel filter. The signals were digitized using an Axon Digidata 1550b analogue-to-digital converter (Axon Instruments Inc.) and acquired using pClamp 10.7 software (Molecular Devices, San Jose, CA, USA, RRID:SCR_011323).

The *in vivo* recordings utilized a similar setup. The ISM was positioned with a manual micromanipulator (Narishige MM-3; Tokyo, Japan) and connected to a dual-channel microelectrode preamplifier (Axoprobe-1A; Axon Instruments Inc.). The ion-barrel signal had the reference signal subtracted from it, and both were amplified 10×. The signals were routed to a Cyberamp 320 signal conditioner (Axon Instruments Inc.) that provided an additional 10× gain and a 2 Hz low-pass 8-pole Bessel filter. The signals were digitized with an analogue-to-digital converter (model USB-6221 M Series DAQ Device, BNC; National Instruments, Austin, TX, USA) and acquired using the custom program WANDA (Odackal *et al.* 2017) written in MATLAB (MathWorks, Natick, MA, USA, RRID:SCR_001622).

Probe transients quantification (PTQ) method

PTQ is a technique that utilizes an ISM along with a molecular probe of the ECS in order to continuously track any transient, relative change in ECS volume (Phillips & Nicholson, 1979; Hansen & Olsen, 1980; Larsen & MacAulay, 2017). We performed this technique to detect and characterize RVP occurring across all models of epileptiform activity in this study. To qualify as an ECS molecular probe, the chosen molecule must be exogenous, able to be dissolved in ACSF, able to have its concentration measured by an ISM, and have negligible toxicity and physiological effects, and cellular uptake on a short timescale (Kaur *et al.* 2008). We used TMA^+ (M.W. 74.14 g/mol) in all experiments except for the experiment where α-naphthalene sulfonate (M.W. 207.23 g/mol) was used.

All *in vitro* PTQ experiments were structured in the following way. First, control ACSF was applied to the mouse brain slice and allowed to equilibrate for 25 min. Next, the ISM recorded the TMA^+ and reference signals 100 μm deep in the slice for 20 min to establish that no volume changes or epileptiform activity were occurring. Chemoconvulsant ACSF was then applied and allowed to equilibrate for 25 min. Meanwhile, the TMA^+ and reference

signals were still being monitored to detect the onset of epileptiform activity. If epileptiform activity began, then the TMA^+ and reference signals were recorded for 20 min. If not, then the slice was discarded, and a new one from the same animal was attempted. These two periods of the experiment—the control ACSF and chemoconvulsant ACSF application periods—were performed for all *in vitro* PTQ experiments. Experiments that incorporated a blocker ACSF underwent a third period comprising 25 min of wash-on and 20 min of recording to determine what effect, if any, the blocker had on epileptiform activity. During each period, the ISM was occasionally brought above the slice to briefly record the TMA^+ signal in the bath (0.5 mM TMA-Cl, Table 1), which was necessary to establish the relationship between recorded voltage and actual TMA^+ concentration.

The *in vivo* PTQ experiments required a different structure because the chemoconvulsant was released locally from a glass micropipette rather than bath-applied. To induce epileptiform activity, a pressure injection micropipette was attached directly to the ISM using dental cement, with the tips placed within 500 μm of each other. The injection micropipette was backfilled with 20 mM (-)-bicuculline methiodide (catalogue #2503, Tocris Biosciences, Bristol, UK) (Xiong *et al.* 2017). Teflon tubing was sealed into the barrel with dental wax and connected to a Toohey Spritzer Pressure System IIe (Toohey Company, Fairfield, NJ, USA). The micropipette array was first placed in the control ACSF continuously flowing over the exposed visual cortex to get a baseline voltage reading on the ISM at a known TMA^+ concentration (1.0 mM TMA-Cl, Table 1). It was then placed several hundred micrometres deep into the visual cortex. After several minutes of recording, a series of short bursts of compressed nitrogen applied to the micropipette containing the convulsant injected small boluses of bicuculline methiodide into the tissue. This was repeated until the ISM detected epileptiform activity. A 20 min period of recording was taken in the region. Afterward, the ISM was retracted into the ACSF above the visual cortex to get another baseline voltage reading.

To analyse the PTQ experiments, 10 min of data from each period (control, chemoconvulsant or blocker ACSF application periods) were used to identify and characterize any RVP that occurred. The periods during which control ACSF was applied never exhibited RVP, so they underwent no further analysis. For the chemoconvulsant ACSF periods, the voltage data were taken from pClamp or WANDA and analysed by a series of custom-built scripts in GNU Octave, version 4.2.2 (available at http://www.octave.org, RRID:SCR_014398). First, the data were converted from voltages into concentrations using the Nicolsky slope and interference of the ISM. Next, the peaks and bases of each individual RVP event were manually identified in order to define each RVP event. Three metrics were calculated from this signal: relative ECS volume shrinkage (amplitude), frequency of RVP, and the sum of areas under pulsations (SAUP).

The relative ECS volume shrinkage per RVP is dependent on the rise in TMA concentration during the pulsation. It was calculated using the following formula:

$$Relative\ ECS\ Volume\ shrinkage\ [\,\%\,] = \left(1 - \frac{\left[TMA^+\right]_{base}}{\left[TMA^+\right]_{peak}}\right) \times 100 \quad (1)$$

Because the magnitude of the relative ECS volume shrinkage is dependent on the amplitude of the RVP events, they are referred to interchangeably in this paper.

The frequency of RVP for all experiments is calculated by taking the number of identified RVP events and dividing by the time period of data recording (i.e. 600 s). Because each RVP event was always accompanied by an event on local field potential (LFP) traces, this metric also reflects the frequency of epileptiform activity on LFP traces. There were never any LFP events that were unaccompanied by an RVP event and vice versa.

The SAUP of the signal was used as a metric to help quantify the total magnitude of volume change events that occurred throughout the data recording period in a way that partially takes into account both the relative ECS volume shrinkage and the frequency. This was calculated by interpolating a local baseline between the base of an RVP event and the point at which the concentration of TMA^+ returns to the concentration at the base. The differences between every point in the signal and the interpolated baseline are calculated and multiplied by the sampling interval, and the results are summed:

$$SAUP = \sum_{i=1}^{n} (C_i - y_i) \times t \tag{2}$$

Where C_i is the TMA concentration of the i^{th} RVP signal, y_i is the TMA concentration of the interpolated baseline, t is the sampling interval, and n is the number of samples in the RVP event. This SAUP analysis was performed on all PTQ experiments that had a pharmacological blocker period. An SAUP ratio between the pharmacological blocker period and the chemoconvulsant period, defined as:

$$SAUP\ ratio = \frac{SAUP_{blocker\ period}}{SAUP_{chemoconvulsant\ period}} \tag{3}$$

was calculated to determine the effect of the blocker on RVP.

To easily compare the RVP data across experiments and determine the effect that any pharmacological blockers have on the frequency of RVP events, Fourier analysis was performed on the TMA concentration signal. The concentration-converted signals were fast-Fourier transformed (fft function from the fftw Octave library), and a power spectrum was evaluated. All frequencies between 0 and 2 Hz (the range of the low-pass filter) were extracted. Because the interval between successive RVP events formed a very low frequency component that we were not interested in analysing, all frequencies below 0.03 Hz were excluded to remove it. The power spectra were then averaged to establish a single spectrum with a frequency resolution of 0.01 Hz.

For all PTQ experiments that did not have a blocker period and underwent this Fourier analysis, the frequency bin with the maximum power was found within the chemoconvulsant ACSF application period of data and the spectrum was normalized to this power. This was done for each individual experiment in a group. A colour map was then constructed grouping the power spectra of all these experiments together. The frequency bins from

the power spectrum of a single experiment were placed on the frequency axis (*y*-axis) of the colour map. The relative power values were assigned colours, ranging from blue (low relative power) to red (high relative power). Each experiment was assigned its own location on the *x*-axis of the map, sorted by frequency of their highest power bin from high to low. One additional column was plotted on each of these maps that took the mean of all the relative powers in a given frequency across all experiments. These represent the 'average' relative power spectrum across all experiments in a group.

The normalization was performed differently for PTQ experiments that had a blocker ACSF application period. Two periods containing RVP comprised each experiment, each with an individual power spectrum to be compared: a 4-AP and a blocker ACSF (containing 4-AP as well, Table 1). The frequency bin with the highest power across either 4-AP or blocker period was identified (i.e. one highest power frequency bin per experiment), and the spectra for both periods were normalized to this power. A colour map was then constructed grouping the power spectra of all of these experiments together. This was done in a similar manner as the colour maps for the PTQ experiments that did not have a blocker ACSF period, except the power spectra belonging to the two periods of each experiment (4-AP and blocker ACSF) were placed next to each other on the *x*-axis. In addition, two 'average' relative power spectra were mapped, one for each period of these experiments.

Real-time iontophoretic (RTI) method

The RTI method is a technique that uses a probe molecule released into the ECS to study the ECS structure (Nicholson & Phillips, 1981). Typically, an iontophoretic microelectrode containing the probe molecule is placed deep in a brain slice, and the molecule is released by application of an electric current into the microelectrode. An ISM sensitive to the probe molecule is placed at a fixed distance from the iontophoretic microelectrode and records the concentration changes of the molecule as it diffuses in the local area. This signal allows for the calculation of two ECS structural parameters. The first, the volume fraction α, is defined as the ratio of the ECS volume to the total tissue volume ($\alpha = V_{ECS} / V_{tissue}$). The second, the diffusion permeability θ, is defined as the ratio of the effective diffusion coefficient of the ECS molecular probe in brain (D^*) to the diffusion coefficient of the same probe in a free medium (D_{free}) ($\theta = D^*/D_{free}$) (Hrabe *et al.* 2004). Diffusion permeability can optionally be converted to tortuosity λ ($\theta = 1/\lambda^2$).

We performed the RTI technique in a standard manner (Odackal *et al.* 2017) on the electrophysiology recording setup used for *in vitro* PTQ experiments. In short, TMA^+ was released from an iontophoretic microelectrode and detected by a TMA-sensitive ISM positioned about 100 μm away. The iontophoretic microelectrode was fabricated out of double-barrelled theta glass (TG200–4; Warner Instruments Corp.). The microelectrode was backfilled with 150 mM TMA-Cl in H_2O in both barrels. Two chloridized silver wires were inserted and sealed in the backfill. TMA^+ ions were released from the iontophoretic microelectrode by applying positive current into the backfill through the chloridized wires. This current was controlled by the pClamp software and digital-to-analogue conversion was provided by the Axon Digidata 1550b. The output analogue signal from the Axon Digidata 1550b was sent to an Axoprobe-1A preamplifier (Axon Instruments Inc.), and

output to the iontophoretic microelectrode using the constant current output feature. The TMA-sensitive ISM was fabricated as described earlier. The RTI experiments started by determining the transport number (n_t), of the TMA-containing iontophoretic microelectrode in a 0.3% agarose gel. The temperature (T) was recorded to control for temperature-induced changes in the diffusion coefficient of TMA^+. A bias current of +20 nA was continuously applied to the iontophoretic microelectrode. Records with duration of 150 s were taken per measurement, during which a step current ranging from +30 nA to +100 nA was applied for a period of 50 s. The recorded signal was analysed using custom MATLAB-based software, WALTER (Odackal *et al.* 2017), in order to extract the transport number (n_t) of the given iontophoretic microelectrode. Afterwards, a brain slice was placed into the submersion tissue chamber, and the ISM and iontophoretic microelectrodes were placed 200 μm deep into the visual cortex of the mouse brain slice 98–122 μm apart. Measurements were taken in the same way as in agarose. The TMA^+ concentration curve was then analysed by WALTER in order to extract α, θ and κ (the non-specific clearance parameter, s^{-1}). Once several measurements were taken under control ACSF conditions, 4-AP ACSF was washed on for 25 min. Any slice that did not exhibit epileptiform activity on the reference signal was discarded. After this 25 min wash-on period, several more RTI measurements were taken under 4-AP conditions. Finally, DIDS (4,4'-diisothiocyano-2,2'-stilbenedisulfonic acid) ACSF was washed on for 25 min and RTI measurements were taken. After recording in brain tissue was completed, the microelectrodes were brought back into 0.3% agarose to check the n_t of the iontophoretic microelectrode. Any experiment in which the n_t before and after the brain measurements changed by more than 10% was excluded.

Statistical analysis

Data are presented as a means ± standard deviation, unless otherwise specified (e.g., as medians with 25th and 75th quartiles). Sample sizes are presented as both n, the number of slices, and N, the number of animals. Power analyses were performed for all experiments using G*Power version 3.0.10 (available at http://www.psychologie.hhu.de/arbeitsgruppen/allgemeine-psychologie-und-arbeitspsychologie/gpower.html). Statistical analysis was performed with SigmaStat (Systat Software Inc, San Jose, CA, USA). A paired t test or Wilcoxon's signed rank test (non-parametric data) was used in the blocker study. Repeated measures ANOVA with Bonferroni *post hoc* testing was used for the RTI data. The significance level was set at $P < 0.05$.

Results

Discovery of RVP in the Has3KO model of epileptiform activity

Our initial observation of RVP occurred while using the PTQ technique (Fig. 1A) in a hippocampal slice from a Has3KO mouse that was immersed in control ACSF containing 0.5 mM TMA^+ (Table 1). In these animals the ECS volume in the stratum pyramidale of the CA1 hippocampus is smaller than in wild-type mice and the slices exhibit spontaneous epileptiform activity along with spontaneous seizures *in vivo* (Arranz *et al.* 2014). The ISM recorded two signals from the stratum pyramidale of the CA1 hippocampus: LFPs where the waveforms indicated spontaneous epileptiform activity (Fig. 1B, top left, blue trace) and

simultaneous changes in TMA^+ concentration that indicated transient ECS volume changes that we call RVP (Fig. 1B, top left, red trace).

Each of these TMA^+ concentration change events can be interpreted as the ECS transitioning back and forth between two states (Fig. 1B, top right). State 1 represents the ECS at a quiescent baseline volume between events. State 2 represents the ECS in a shrunken state, indicated by higher TMA^+ concentration. RVP pulses have a fast-rising phase from state 1 to state 2 that is concurrent with epileptiform activity seen on the LFP trace and typically takes less than a second, and a slower falling phase from state 2 back to state 1. The TMA^+ concentration monitors in real time how the ECS is shrinking and expanding back to a baseline volume every time an epileptiform waveform occurs in the LFP trace. We regularly observed RVP in the stratum pyramidale of the CA1 hippocampus in slices taken from Has3KO mice (n = 10 slices, N = 10 animals). In all recordings, each epileptiform event on the LFP trace was accompanied by an RVP event and vice versa. This activity persisted for as long as we recorded, as shown in a representative recording taken over a period of 2 h (Fig. 1B, bottom).

RVP occurs in a variety of models of epileptiform activity *in vitro*

After the initial observation of RVP in the Has3KO, we asked whether this phenomenon would occur in other models of epileptiform activity. We also wanted to make sure RVP could be detected with an ECS molecular probe other than the TMA^+.

The first model of epileptiform activity employed a bath application of Picrotoxin (50 μM, Loucif *et al*. 2005), a $GABA_A$-receptor inhibitor that induces epileptiform activity *in vitro* and *in vivo*. This is an acute model that has been shown to elicit SES (Olsson *et al*. 2006; Tønnesen *et al*. 2018). We applied the PTQ technique (Fig. 2A) in the slices undergoing picrotoxin-induced epileptiform activity and used two different ECS molecular probes in two PTQ experiments. The cation TMA^+ (Fig. 2B, top traces) is the most commonly used small cationic ECS molecular probe while α-naphthalene sulfonate (α-NS^-) (Fig. 2B, bottom traces) is a small anionic molecular ECS probe (Nicholson & Phillips, 1981). Both recordings revealed similar RVP events to those in the Has3KO experiment (n = 9 slices, N = 9 animals for TMA^+, the stratum pyramidale of the CA1 hippocampus or visual cortex; n = 4 slices, N = 4 animals for α-NS, visual cortex). This suggested that RVP also occurs in a pharmacological model of epileptiform activity and that the TMA^+ findings were truly reflective of the ECS volume changes.

We next investigated two additional models of epileptiform activity: bicuculline, a $GABA_A$-receptor antagonist, and 4-AP, a blocker of voltage-gated K^+ channels. Bicuculline is another model of epileptiform activity commonly used *in vitro* and shares a similar mechanism of action to picrotoxin. We used the PTQ technique with the TMA^+ probe in the visual cortex of brain slices. One set of slices was treated with bicuculline (50 μM, Lee *et al*. 2002) and the other with 4-AP (100 μM, Salah & Perkins, 2011); the resulting TMA^+ and LFP signals are shown in Fig. 2C. Both chemoconvulsants produced waveforms on LFP traces indicating epileptiform activity and RVP (n = 4 slices, N = 4 animals for bicuculline; n = 60 slices, N = 48 animals for 4-AP). Data obtained with several chemoconvulsants,

together with our results in Has3KO mice, show that the generation of RVP is not limited to a particular mechanism for generating epileptiform activity.

RVP occurs in the bicuculline methiodide model of epileptiform activity *in vivo*

We next sought to confirm the presence of RVPs in an *in vivo* model. An *in vivo* system differs from a brain slice; most obviously a whole brain has intact circulation that alters the clearance and fluid dynamics of the ECS in comparison to slices (Hrabetova & Nicholson, 2007; Xie *et al*. 2013). We set up the PTQ technique as shown in Fig. 2D. Bicuculline methiodide was chosen as the model of epileptiform activity for the *in vivo* preparation. We used this chemoconvulsant because of technical difficulties with our first-choice model, the 4-AP: at the concentration we needed to induce epileptiform activity in the *in vivo* preparation, the 4-AP disrupted the TMA-ISM functionality. Recording from the visual cortex *in vivo* after bicuculline methiodide application revealed LFP waveforms indicating epileptiform activity (Fig. 2E, blue trace). The TMA^+ signal documented the presence of RVP in an *in vivo* system (Fig. 2E, red trace) ($N = 5$ animals).

Quantification of epileptiform activity and RVP in *in vitro* and *in vivo* models of epileptiform activity

After establishing the ubiquity of the RVP phenomenon across several models of epileptiform activity, we wanted to quantify the frequency and amplitude of the RVP events, together with the frequency of epileptiform activity. We employed the PTQ technique to study the epileptiform activity and RVP induced by 4-AP *in vitro*, and by bicuculline methiodide *in vivo*. The 4-AP *in vitro* model was chosen because it is well established and, at the concentration that produces epileptiform activity *in vitro* (100 μM), it does not interfere with the ISM recording.

After the 4-AP ACSF was washed on brain slices, the ISM recorded epileptiform activity and RVP events (Fig. 3A). Ten minutes of recording during the 4-AP ACSF period were extracted and three metrics were evaluated (Fig. 3B): the frequency of epileptiform activity, the RVP frequency, and the RVP amplitude that provided relative ECS volume shrinkage (eqn 1). We found that the average frequency of both the epileptiform activity and the RVP events was 0.11 ± 0.06 Hz ($n = 60$ slices, $N = 48$ animals; Fig. 3C, top), with the highest frequency reaching 0.32 Hz. In all recordings, each epileptiform event on the LFP trace was consistently accompanied by an RVP event and vice versa. The average relative ECS volume shrinkage was 4.4% ± 3.1% (Fig. 3C, bottom), with the highest shrinkage reaching 16.3%. To visualize the RVP periodicities across experiments, a power spectrum of a 10 min period of the TMA^+ concentration signal from each experiment was generated and displayed in a colour map (Fig. 3D). We found that frequency components were dominated by slower RVP activity (0.03 Hz). However, in several experiments the RVPs were dominated by higher frequencies (about 0.15–0.25 Hz).

In the bicuculline methiodide *in vivo* model, we found the average frequency of both the epileptiform activity and the RVP events of 0.35 ± 0.18 Hz ($N = 5$ animals; Fig. 3E, top), with the peak frequency of 0.58 Hz. Again, each epileptiform event on the LFP trace was accompanied by an RVP event and vice versa. The average relative ECS volume shrinkage

was 14.8% ± 8.3% (Fig. 3E, bottom), with the largest shrinkage reaching 27.4%. The generated power spectra (Fig. 3F) show that on average the RVP occurred at very low frequencies (under 0.1 Hz) but there were some experiments with much more frequent events (around 0.5 Hz).

In summary, the RVP events occur in conjunction with the epileptiform events both *in vitro* and *in vivo*. During RVP, the ECS transiently shrinks by more than 4% *in vitro* and by almost 15% *in vivo*.

First phase of the search for mechanism: NKCC1, KCC2 and AQP4 blockade does not inhibit RVP in the 4-AP model *in vitro*

We next investigated the blockers of channels and transporters to determine their effects on RVP and epileptiform activity. To this end, we employed a two-phase study design (Figs 4A, B) that allowed us to eliminate drugs unlikely to significantly affect RVPs in the first phase, and then investigate in more detail the effects of the remaining drugs in the second phase. Both phases relied on PTQ to compare the RVP events recorded during two experimental periods: a 4-AP ACSF application period, and a 4-AP + channel/transporter blocker ACSF application period. We employed the *in vitro* model for the entire two-phase study because brain slices offer more precise distribution of bath-applied pharmacological agents than surface application in the whole brain does (Hrabetova & Nicholson, 2007).

During phase 1 of our study, we filtered our initial pool of candidates according to their ability to reduce the SAUP ratio of the RVP (eqns 2 and 3). The SAUP ratio metric is sensitive to both amplitude and frequency of the RVP (Fig. 4C). This phase required small sample sizes ($n = 5$ slices from $N = 5$ animals per group, eight groups) because it merely searched for candidates with the largest effect on the RVP.

To demonstrate that 4-AP-induced activity and RVP would not terminate spontaneously during the time period we apply blockers, we also performed a control experiment in which a slice was only exposed to 4-AP ACSF (Fig. 4D). The left trace corresponds to the time period of a typical 4-AP recording (i.e. 35 min after wash-on), while the right trace corresponds to the time period of a typical blocker recording (i.e. 35 min following the 4-AP recording period).

The first transporters we targeted, NKCC1 and KCC2, are found on neurons in adult animals and can transport large amounts of osmolytes and water across the cell membrane. We screened a family of drugs comprised of furosemide (NKCC1 and KCC2 blocker), bumetanide (NKCC1 blocker) and VU0463271 (KCC2 blocker) (Fig. 4A, left). Traces taken during furosemide application (2.5 mM, Hochman 2012; Fig. 4E) showed a reduction in events occurring in both the TMA^+ concentration and in the LFP traces. Following furosemide application, the SAUP ratio was significantly reduced in comparison with the control value in 4-AP ACSF (Fig. 4F; 0.0186 ± 0.0277, $P < 0.0001$, paired t test). Even when tested at a lower concentration (1 mM), there was a prominent decrease (Fig. 4F; 0.254 ± 0.185, $P = 0.0008$, paired t test). However, this extreme effect of furosemide was not reproduced when using a combination of the two specific blockers for NKCC1 and KCC2, bumetanide (10 μM, Hochman, 2012) and VU0463271 (10 μM, Sivakumaran *et al.* 2015)

(Fig. 4F; 0.787 ± 0.345 $P = 0.240$, paired t test). We also tested bumetanide alone and VU0463271 alone. Bumetanide did not have a significant effect on the SAUP ratio (Fig. 4F; 1.098 ± 0.333, $P = 0.547$, paired t test) while VU0463271 significantly reduced the SAUP ratio (Fig. 4F; 0.521 ± 0.141, $P = 0.002$, paired t test). Based on these data, furosemide (that blocks both NKCC1 and KCC2) was excluded from further consideration in phase 2 because a combination of bumetanide (that blocks NKCC1) and VU0463271 (that blocks KCC2) did not replicate its effect. We suspect that furosemide may act on additional targets that are currently not identified. We also excluded VU0463271 because additional analysis revealed that this blocker increased the frequency of epileptiform activity recorded on the LFP traces by 61.4% (4-AP: 0.101 ± 0.064 Hz, 4-AP + VU 0463271: 0.163 ± 0.072; $P = 0.048$, paired t test). The frequency of concomitant RVP events was also increased, by 61.4%, but their amplitude was smaller, resulting in a decreased SAUP ratio. We therefore concluded that neuronal NKCC1 and KCC2 transporters were not necessary for RVP generation during 4-AP-induced epileptiform activity.

Because astrocytes are usually thought of as the cell type that most readily swells during neuronal hyperexcitability (Dietzel *et al.* 1989; Murphy *et al.* 2017*a*), we next investigated several channels and transporters found on these cells. Blockers of these channels and transporters—TGN-020 (31 μM, AQP4 blocker, Huber *et al.* 2009; Toft-Bertelsen *et al.* 2020), $BaCl_2$ (100 μM, Kir4.1 blocker, Larsen *et al.* 2014) and DIDS (4,4'-Diisothiocyano-2,2'-stilbenedisulfonic acid, 300 μM, NBCe1 blocker, Larsen & MacAulay, 2017) (Fig. 4A, right)—were applied in the visual cortex *in vitro* where 4-AP induced RVP and epileptiform activity. Application of 4-AP + TGN-020 ACSF produced no effect on the SAUP (Fig. 4G; 1.149 ± 0.260, $P = 0.269$, paired t test), 4-AP + $BaCl_2$ ACSF showed the second largest effect (Fig. 4G; 0.541 ± 0.209, $P = 0.008$, paired t test) and 4-AP + DIDS ACSF showed the greatest effect, with almost complete elimination of the RVP during its application (Fig. 4G; 0.0060 ± 0.0046, $P < 0.0001$, paired t test), in comparison with their respective values in 4-AP. Based on these results, $BaCl_2$ and DIDS were chosen for phase 2 of the blocker study while TGN-020 was not investigated further.

In summary, analyses employed in phase 1 identified $BaCl_2$ and DIDS as the blockers promising to reduce or eliminate the generation of RVP during epileptiform activity through their intended targets.

Second phase of the search for mechanism: NBCe1 blockade suppresses RVP in the 4-AP model *in vitro*

Phase 2 of the study investigated the remaining candidate blockers based on the SAUP ratio (eqns 2 and 3), the relative ECS volume shrinkage (eqn 1) and the frequency of RVP (Fig. 5A). A blocker that caused a statistically significant reduction in the SAUP, decreased both the amplitude and frequency metrics, and overall reduced the power of all frequency components of the RVP, was deemed to inhibit RVP generation. We also evaluated the frequency content of epileptiform activity to determine whether a blocker inhibited it (Fig. 5A). Phase 2 used larger sample sizes ($n = 10$ slices from $N = 10$ animals per group, two groups) to identify the blockers with robust effects on RVP and epileptiform activity.

The blockers of Kir4.1 and NBCe1 were both tested in phase 2 using the PTQ technique on the 4-AP model *in vitro*, with a similar experimental protocol to that used in phase 1. Both $BaCl_2$ (100 μM) and DIDS (300 μM) significantly reduced the SAUP during their application ($BaCl_2$: 0.610 ± 0.352, $P = 0.007$, paired t test; DIDS: median was 0.000, 25% quartile was 0.000, 75% quartile was 0.000, $P = 0.002$, Wilcoxon's signed rank test), with DIDS having the largest effect (Fig. 5B).

The decrease in the SAUP induced by $BaCl_2$ and DIDS could have resulted from uniform changes in amplitude and frequency (i.e. both were reduced) or from opposite effects on each (e.g. low amplitude, but high frequency). Furthermore, the SAUP does not describe comprehensively what happened to the epileptiform activity during blocker application, making analysis of the frequency necessary. Therefore, we calculated the ratio of average amplitude and frequency of RVP during the 4-AP + blocker period to the amplitude and frequency during the 4-AP only period. We also calculated the ratio of the frequency of epileptiform activity during the 4-AP + blocker period to the frequency during the 4-AP only period. This analysis revealed that $BaCl_2$ exhibited a mixed effect: it quelled the amplitude of the RVP events (0.483 ± 0.249, $P = 0.0001$, paired t test) but made them more frequent (median was 1.83, 25% quartile was 1.58, 75% quartile was 3.48, $P = 0.002$, Wilcoxon's signed rank test) (Fig. 5C, left). The frequency of epileptiform activity in 4-AP + $BaCl_2$ was significantly increased in comparison with its values in 4-AP (Fig. 5C, right; median was 1.83, 25% quartile was 1.58, 75% quartile was 3.48, $P = 0.002$, Wilcoxon's signed rank test). In contrast, DIDS suppressed both RVP metrics (amplitude: median was 0.000, 25% quartile was 0.000, 75% quartile was 0.000, $P = 0.002$, Wilcoxon's signed rank test; frequency: median was 0.000, 25% quartile was 0.000, 75% quartile was 0.000, $P = 0.002$, Wilcoxon's signed rank test), virtually eliminating them (Fig. 5C, left). The frequency of epileptiform activity in 4-AP + DIDS was also suppressed (Fig. 5C, right; median was 0.000, 25% quartile was 0.000, 75% quartile was 0.000, $P = 0.002$, Wilcoxon's signed rank test).

Another way to determine the effect of blockade was to compare the average power spectra of the RVPs between the application periods of 4-AP ACSF and blocker ACSF. This time, each experiment involved two power spectra: one corresponding to the 4-AP ACSF period (columns labelled 'A' in Figs. 5D, E) and one corresponding to the blocker ACSF period (columns labelled 'B' in Figs 5D, E). The colour map for $BaCl_2$ (Fig. 5D) supports the RVP amplitude and frequency breakdown in Fig. 5C. Almost all experiments have their frequency component with the highest relative power shifted to a higher frequency, but their overall power is almost uniformly lower; this trend is evident in the 'average' columns (Fig. 5D, right). The colour map corresponding to DIDS (Fig. 5E) also matches the data from Fig. 5C. All experiments show reduction in overall power, to the point where any trace of the RVP signal almost completely disappears. This trend is very apparent in the 'average' columns (Fig. 5E, right).

In summary, analyses employed in phase 2 identified DIDS as the blocker that profoundly inhibits the generation of RVP and epileptiform activity.

NBCe1 blockade by DIDS reverses the SES induced by 4-AP epileptiform activity *in vitro*

Because the blockade of NBCe1 with DIDS virtually eliminated both RVP and epileptiform activity, we also investigated the effect that DIDS has on the SES in a 4-AP *in vitro* model of epileptiform activity. Our hypothesis was that DIDS reversed the SES of the ECS during epileptiform activity, allowing the ECS to recover to its normal size. Furthermore, we wanted to quantify the SES in the 4-AP *in vitro* model. We employed the RTI technique in the visual cortex of a mouse brain slice (Fig. 6A) to measure the absolute ECS volume fraction α. The RTI measurements were taken during three periods: the control period (Fig. 6B, left), the 4-AP period (Fig. 6B, middle) and the 4-AP + DIDS period (Fig. 6B, right).

The RTI measurements of ECS volume fraction α under these three conditions showed that 4-AP induced a SES similar to those described in the literature for other chemoconvulsants (Lux *et al.* 1986; Slais *et al.* 2008; Tønnesen *et al.* 2018) and that 4-AP + DIDS ACSF application reversed the 4-AP-induced SES (Fig. 6C, left). Control conditions showed an α of 0.25 ± 0.03 while the 4-AP condition revealed an α of 0.16 ± 0.03 (n = 10 slices from N = 10 animals per group, P = 0.000008, repeated measures one-way ANOVA with Bonferroni *post hoc* testing), representing a 36% reduction of the ECS volume. Following 4-AP + DIDS ACSF application, α rose to 0.29 ± 0.05, which was 82% higher than the 4-AP condition (n = 10 slices, N = 10 animals for 4-AP; n = 5 slices, N = 5 animals for 4-AP + DIDS; P = 0.000002, repeated measures one-way ANOVA with Bonferroni *post hoc* testing) and 16% higher than the control condition (P = 0.034, repeated measures one-way ANOVA with Bonferroni *post hoc* testing). The diffusion permeability θ did not significantly change throughout any of the conditions (control: 0.392 ± 0.056, 4-AP: 0.372 ± 0.059, 4-AP + DIDS: 0.322 ± 0.044; P = 0.06, repeated measures one-way ANOVA) (Fig. 6C, right). The non-specific clearance parameter κ was significantly lower in the 4-AP + DIDS condition than in the 4-AP condition (control: 0.011 ± 0.006 s^{-1}, 4-AP: 0.016 ± 0.008 s^{-1}, 4-AP + DIDS: 0.006 ± 0.004 s^{-1}; P = 0.013, repeated measures one-way ANOVA; P = 0.105 for control *vs.* 4-AP, P = 0.018 for 4-AP *vs.* 4-AP + DIDS, P = 0.464 for control vs. 4-AP + DIDS, Bonferroni *post hoc* testing).

In summary, DIDS reversed the SES and resulted in an increased ECS volume following blockage of epileptiform activity and RVP.

Discussion

To the best of our knowledge, this is the first report of the RVP phenomenon. There are three main results. First, we established that RVPs commonly occurred in several models of epileptiform activity both *in vitro* and *in vivo*. Second, quantitative analysis determined that the individual RVP pulses shrank ECS volume by more than 4% *in vitro* and by almost 15% *in vivo*. Third, we found that the pharmacological blockage of the electrogenic Na^+/HCO_3^- cotransporter NBCe1 by DIDS eliminated the RVP, the SES and the epileptiform activity. We conclude that RVP underlies epileptiform activity in mice, and that NBCe1 is likely linked to the generation of RVPs, SES and epileptiform activity. We argue that inhibition of the ECS volume changes may represent a target worthy of exploration in patients suffering from epilepsy which is resistant to current treatments.

The relationship between RVP and SES

If the ionic imbalances occurring during epileptiform events cause the ECS to contract (Lux et al. 1986), RVP events should always be observed accompanying such epileptiform events. However, while several previous studies have observed SES in several seizure models, RVP has not been previously identified, probably because of low temporal resolution of the methods used in these studies. In the original study that reported ECS shrinkage during epileptiform activity, a TMA-based method was used that required over 10 s to make a measurement (Dietzel *et al.* 1980). In that period, neurons would have fired many times, but the value extracted would be an average of the ECS volume during that period and would not reveal second-to-second changes in ECS volume. Other techniques that have been used to measure SES in models of epileptiform activity and seizures also have a low temporal resolution; these techniques include RTI (Slais *et al.* 2008) and super-resolution shadow imaging (Tønnesen *et al.* 2018). The tissue-resistance measurements used in models of epileptiform activity by Traynelis and Dingledine (1989) are fast enough to record RVP, requiring 5–15 ms for a single measurement, but RVP was not reported. This may have been because the investigators averaged measurements across many events of epileptiform activity or because they disregarded any measurements that were taken during interictal bursts or population spikes, which is the time of peak RVP. Therefore, the data of Traynelis and Dingledine likely reflect measurement of SES.

The PTQ technique has been used to measure ECS shrinkage during spreading depression (Phillips & Nicholson, 1979), ischaemic depolarization (Hansen & Olsen, 1980) and neuronal stimulation (Larsen & MacAulay, 2017). However, PTQ cannot detect SES because the ECS molecular probe used for measuring relative volume changes slowly equilibrates with the surrounding undisturbed probe population through diffusion. Therefore, the technique is limited to measuring rapid volume changes (Hansen & Olsen, 1980). To measure RVP and SES, both the PTQ and the RTI techniques are required.

Prior reports of the SES during epileptiform activity and seizures reported ECS volume shrinkage of roughly 35% (Lux *et al.* 1986; Slais *et al.* 2008; Tønnesen *et al.* 2018). However, these values are likely an average of the overall volume of the ECS during the length of the measurement. For instance, Slais *et al.* (2008) reported an SES that reached 32% shrinkage during peak intensity of pilocarpine-induced status epilepticus. The RTI method was used to make these measurements, so one measurement probably took at least 50 s. Based on our findings, the ECS is likely exhibiting not just an SES during such measurements but also an RVP that further influences the ECS volume. In light of the RVP discovery, it is useful to separate the RVP and SES components. Therefore, we took RTI measurements in the 4-AP model to measure the SES during our recordings and found a similar average volume change (36% drop). Our *in vitro* measurements of RVP showed they shrink the ECS by an additional 4.4% on average, reaching a maximum of 16.3%. Because the RVP is occurring in an ECS that also underwent SES, the RVP shrinkages are relative to the already reduced ECS volume fraction, 0.16, typically found during an SES. This means that the ECS volume fraction α at the peak of an average RVP is 0.153 (4.4% less than 0.16) and can fall to 0.134 (16.3% less than 0.16) for the largest RVP in the *in vitro* model. We can make a prediction for the *in vivo* model even though we do not have RTI measurements

there, because the magnitude of *in vivo* SES reported in the literature (Slais *et al.* 2008) was similar to our *in vitro* SES measurement. The RVP we measured *in vivo* shrank the ECS by 14.8% on average, with a maximum of 27.4%. This means that in the *in vivo* model, the ECS volume fraction α is likely to reach 0.136 (14.8% of 0.16) at the peak of an average RVP, and 0.116 at the peak of the largest RVP. This large impact of RVP on the ECS volume during epileptiform activity highlights its importance.

Which cells swell to produce RVP and SES?

To generate an SES or RVP, water must move from the ECS into cells, causing them to swell. It is unclear, however, if water swells astrocytes selectively, or if it enters neurons as well. Previous studies of activity-induced volume changes imply that astrocytes swell and that this water transport depends on the activity of specific astrocytic transporters NBCe1 and H^+-coupled monocarboxylate transporter (MCT) 1 and 4 (Larsen & MacAulay 2017; MacAulay 2020). Our data suggest that NBCe1 is necessary for the generation of RVP and SES, implying that astrocytes swell during such volume changes.

Neurons have been shown to resist volume changes under physiological conditions but there is evidence that pathological conditions can trigger such changes. Modest elevations in $[K^+]_{ECS}$ (Walch *et al.* 2020) or hypoosmolar challenges (Andrew *et al.* 2007) have been shown to induce astrocytic-selective swelling, although there are some competing observations (Murphy *et al.* 2017*b*). It is accepted, however, that neurons swell in pathological situations, such as oxygen-glucose deprivation (Andrew *et al.* 2007) and excitotoxicity (Rungta *et al.* 2015). In hyperexcitable states, such as cortical spreading depression and seizures, this swelling occurs concurrently with large alterations in ionic balance (Steffensen *et al.* 2015, Sword *et al.* 2017, Glykys *et al.* 2019) but it is unclear whether ionic disruption is the direct cause of the neuronal swelling (Larsen *et al.* 2019). Our findings implicate astrocytes and suggest that astrocytic swelling is likely a large contributor to RVP and SES. However, neuronal swelling warrants further investigation.

Transporters and channels that do not support RVP and epileptiform activity generation

Our blocker study was guided by a simple question: how does the water leave the ECS to generate RVP? The first phase allowed us to eliminate the NKCC1/KCC2 transporters and AQP4 from the list of components necessary for RVP and epileptiform activity generation. The lack of effect of bumetanide + VU0463271 implies that NKCC1/KCC2 transporters are not involved, and the large effects of furosemide are likely attributed to its activity on other transporters (Uwera *et al.* 2015). We also determined that blockade of AQP4 by TGN-020 had no effect on epileptiform activity or RVP generation. These results agree with previous studies testing the role of AQP4 channels in the ECS shrinkage during stimulus-evoked neuronal activity. Neither genetic removal of AQP4 channels in mice (Haj-Yasein *et al.* 2012) nor the pharmacological blockage with a specific inhibitor TGN-020 (Toft-Bertelsen *et al.* 2020) prevented the shrinkage of ECS.

Blockade of the Kir4.1 channel led to the reduction of RVP magnitude in the first phase of our study, but the second phase revealed a more complicated effect on epileptiform activity and RVP. The $BaCl_2$-induced blockade of Kir4.1 elicited sufficient inhibition of RVP to

consider it a candidate for further examination, which showed that the volume changes were decreased in amplitude but increased in frequency. This was directly reflected in the frequency of epileptiform waveforms on LFP traces, indicating that the epileptiform activity was more frequent as well. A previous study found that application of $BaCl_2$ had no effect on activity-induced shrinkage of ECS (Larsen *et al.* 2014) while our study showed that it resulted in an increase of epileptiform activity. We note that, although $BaCl_2$ is used as a Kir4.1 blocker, it also acts on other potassium channels. For example, $BaCl_2$ was reported to have a bidirectional effect on BK channels where an initial transient activation was followed by a steady-state block that persisted beyond the washout of $BaCl_2$ (Zhou *et al.* 2012). In general, BK channels are involved in reducing neuronal excitability and their blockage can trigger epileptic seizures (N'Gouemo 2011). In our study of 4-AP-induced epileptiform activity, the detailed analysis of $BaCl_2$ effects on epileptiform activity and RVP revealed that the frequency of epileptiform activity and RVP increased. This effect may result from the block of BK channels with $BaCl_2$. One possible explanation for the reduction of RVP amplitude during $BaCl_2$ application is that the ECS is being sustained in a more constricted state. It may then be harder to produce large and fast changes in the ECS volume when it is already constricted.

NBCe1 transporter supports RVP and epileptiform activity generation

A recent study of the role of the NBCe1 transporter in activity-induced shrinkage of the ECS (Larsen & MacAulay, 2017) informed our hypothesis about the role of NBCe1 in RVP generation. That study used the PTQ technique along with pH-sensitive and K^+-sensitive ISMs to investigate ECS changes in the hippocampus after stimulation of the Schaffer collaterals in a mouse brain slice. The investigators reported that during neuronal firing the ECS volume shrinks, pH_{ECS} becomes rapidly alkaline and subsequently slowly acidifies, and $[K^+]_{ECS}$ increases–all on a similar timescale. After washing on DIDS (300 μM) to block NBCe1 running in a reversed mode due to astrocytic depolarization, they noted that the reduction of ECS volume was smaller and the alkaline shift was larger, but the $[K^+]_{ECS}$ was unaffected. This work has implications for our study because the activity-induced ECS shrinkage is a similar phenomenon to the epileptiform activity-related RVP, and the results of DIDS application in our 4-AP model may thus correspond to what Larsen and MacAulay saw in their model. All three metrics that they evaluated had the potential to modulate neuronal excitability but in different ways: less ECS shrinkage would cause less excitability, higher pH_{ECS} would cause more excitability (Sinning & Hübner, 2013), and maintaining the same $[K^+]_{ECS}$ transient would not alter excitability. If alkalization was the dominant consequence of NBCe1 blockade in our study, we would expect to see enhancement of epileptiform activity (Velíšek et al. 1994; Sinning & Hübner, 2013) and concomitant enlargement of RVP, but this is not what we found. On the other hand, if counteracting the ECS shrinkage was the dominant consequence, we would expect to see suppression of epileptiform activity because enlarged ECS volume decreases neuronal excitability and ephaptic interactions. Indeed, our study showed that both RVP and epileptiform activity were obliterated by NBCe1 blockade, making it more likely that the epileptiform activity was halted due to DIDS-induced reversal of ECS shrinkage rather than changes to pH.

In addition to investigating the effect of DIDS on RVP, we also investigated its effect on SES using the RTI method. Based on our hypothesis that DIDS prevents ECS shrinkage during 4-AP application, it was expected that the ECS volume after DIDS application would return to control (pre-4-AP) values because the blockade of NBCe1 transporter should inhibit the movement of osmolytes into the astrocytes following their depolarization. Our finding that ECS volume increases in the 4-AP condition after DIDS application suggests that it may be exerting its inhibiting effects on epileptiform activity through modulation of the extracellular volume.

DIDS has been used to reduce the frequency of seizures and modify vasogenic oedema caused by status epilepticus (Yang *et al.* 2017). Cytotoxic oedema caused by blood–brain barrier dysregulation is one of the negative consequences of hyperexcitable states, specifically status epilepticus (Jo *et al.* 2011). Yang *et al.* (2017) investigated chronic intraventricular DIDS administration in an *in vivo* rat lithium-pilocarpine model of temporal lobe epilepsy and demonstrated that DIDS attenuated vasogenic oedema and prevented neuronal loss in the piriform cortex following status epilepticus. The treatment also resulted in a reduction in seizure frequency and severity, even following discontinuation of treatment. The authors attributed the antiepileptic effects to DIDS preventing tight junction protein disruption at the blood–brain barrier in their seizure model. While this confirms the possible clinical relevance of DIDS in the treatment of seizures, the blood–brain barrier modification effect is unlikely to be the mechanism of epileptiform activity inhibition in the 4-AP *in vitro* model because leakage of fluid across the blood–brain barrier is not possible in a brain slice. An *in vitro* model of intracellular oedema (Kumar *et al.* 2006) revealed that DIDS eliminated the formation of cellular oedema in slices treated with NMDA to induce excitotoxicity but had no effect on slices undergoing oxygen-glucose deprivation. This indicates that DIDS can modify fluid dynamics specifically during an excitable state. It also provides support for the involvement of NBCe1 in the inhibiting effect of DIDS on epileptiform activity because NBCe1 reverses to cotransport Na^+ and HCO_3^- inward during astrocytic depolarization (Deitmer & Szatkowski, 1990; Theparambil *et al.* 2014, 2015; Larsen & MacAulay, 2017). Although we argue for NBCe1 being the main target for inhibition of epileptiform activity, it is possible that the inhibition is due to another target blocked by DIDS, such as Na-independent Cl^-/HCO_3^- exchangers (AE-family) (Ringel *et al.* 2001) or voltage-gated chloride channels (CLC-family) (Wu *et al.* 2019). However, knock-out mice that are deficient in AE3, a member of the AE family, are prone to developing idiopathic seizures (Hentschke *et al.* 2006; Parker, 2018), which makes this transporter an unlikely target contributing to the epileptiform activity inhibition of DIDS. Furthermore, in a recent study by Onodera *et al.* (2021), pharmacological blockade of NBCe1 with a different drug, S0859, blocked development of the increase in neuron hyperexcitability that occurs after a period of epileptiform activity in the mouse hippocampal slice, and blocked the growth in afterdischarge duration and kindling acquisition in the mouse hippocampal kindling model. These results suggest that blockade of NBCe1 can have an antiepileptogenic as well as an antiepileptic effect. While the large effect of DIDS on ECS volume and on epileptiform activity should not be ignored, it is not yet known what DIDS does to the extracellular volume under normal conditions, and whether it prevents seizures.

The relationship between ECS volume changes (RVP and SES) and epileptiform activity

We found that epileptiform activity *in vitro* and *in vivo* is accompanied by RVP, a new type of volume change distinct from SES (Lux *et al*. 1986; Slais *et al*. 2008; Tønnesen *et al*. 2018). We propose that ECS shrinkage during RVP, similarly to SES, is a consequence of neuronal activity. In turn, ECS shrinkage facilitates hyperexcitability and synchrony by increasing the extracellular concentration of neuroactive substances (Andrew & MacVicar, 1994; Kilb *et al*. 2006) and by enhancing ephaptic interactions between depolarizing cells (Dudek *et al*. 1986; Weiss & Faber, 2010). Through its effect on ECS volume, RVP may contribute to sustaining neuronal hyperexcitability and synchrony, keeping the neuronal network running in a positive feedback loop of perpetual activity and preventing a return to its physiological state.

Based on our study and the literature, SES and RVP are common in several models of epileptiform activity and seizures. It is unknown whether a seizure can develop without any ECS shrinkage. In our study, RVP, SES and epileptiform activity were all linked together; any blockers that inhibited RVP, such as DIDS, also inhibited epileptiform activity. Notably, DIDS also inhibited SES. We consider it most likely that DIDS suppresses epileptiform activity by inhibiting ECS shrinkage, which in turn inhibits both SES and RVP; the link between ECS shrinkage and epileptiform activity has support from the literature (for review, see Murphy *et al*. 2017*a*; Colbourn *et al*. 2019). Prior studies have shown that blockade of the SES is a viable strategy for treatment of seizures (for review, see Murphy *et al*. 2017*a*). We have identified RVP as an additional component in the ECS volume changes during epileptiform activity. We believe its recognition will be important for an accurate description of the abnormal neuronal activity and may present a suitable target for seizure inhibition.

It is difficult to establish a clear causal relationship between the RVP, SES and epileptiform activity. This is an inherent problem of not only our experimental design but also possibly the nature of the phenomenon under investigation. If there is a circular dependency of ECS shrinkage and epileptiform activity, an inhibition of one will invariably affect the other. Now that DIDS has been identified as a blocker of interest, future studies can be directed to addressing this problem.

Conclusions

Epileptiform activity induces a previously undescribed ECS dynamism that we call RVP. We hypothesized that the RVP and epileptiform activity could be stopped by blocking transporters involved in substantial water movement, or those involved in K^+ transport. We found that blockade of transporters NKCC1/KCC2, or blockade of the AQP4 channel, did not inhibit RVP. Blockade of Kir4.1 partially inhibited it while worsening the epileptiform activity. The main inhibition of RVP and epileptiform activity was achieved by blockade of NBCe1, a transporter that is known to be involved in activity-induced shrinkage of the ECS. Its blockade impeded both the ECS volume changes (RVP and SES) and the epileptiform activity.

Supplementary Material

Refer to Web version on PubMed Central for supplementary material.

Acknowledgements

The authors would like to thank Dr Yu Yamaguchi at Sanford Children's Health Research Center, Sanford Burnham Prebys Medical Discovery Institute, La Jolla, California for providing the Has3KO animals; Dr Jeremy Weedon for assistance in designing the two-phase study and statistical analysis; Dr Richard Kollmar for providing edits and suggestions for the manuscript; Aditi Naik for providing assistance during some of the experiments and assisting in early edits of the manuscript.

Funding

This work was supported by National Institutes of Health National Institute of Neurological Disorders and Stroke grants R56 NS047557 and R01 NS047557 (principal investigator Dr Sabina Hrabetova), National Institutes of Health National Institute of Aging grant RF1 AG057579 (principal investigator Dr Yu Yamaguchi), National Institutes of Health National Institute of Neurological Disorders and Stroke grant R01 NS088496 (principal investigator Dr Yu Yamaguchi), NYS Office of People with Developmental Disabilities (OPWDD) fellowship (Robert Colbourn). Parts of this work have previously been reported in conference abstracts.

Biography

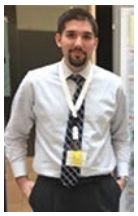

Robert Colbourn is currently an MD/PhD student at SUNY Downstate Health Sciences University. He received a BS in Biology and Chemistry at Brooklyn College. He completed his PhD in the Neural and Behavioral Sciences Program at SUNY Downstate, where he studied the dynamics of the brain's extracellular space during epileptiform activity in the labs of Dr Sabina Hrabetova at SUNY Downstate, and Dr Jeffrey Goodman at the New York State Institute for Basic Research.

Data availability statement

All data points are available: 1) for $n < 30$, all data points are plotted within the figures in the manuscript, 2) for $n > 30$, data are also provided as supporting information.

Appendix

Our experiments show that RVP events happen concurrently with the events of epileptiform activity and vice versa. When we discovered RVP, we questioned whether the phenomenon is an artefact related to the PTQ technique or the ECS molecular probe used in our study. To address this concern, we performed the analyses and experiments described in this Appendix.

RVP phenomenon is real

First, we briefly summarize how the voltages measured with a double-barrelled ISM are processed (Fig. 7A). The barrel containing the ion exchanger (ion-selective barrel) measures a voltage V_1 which has two components. The first component is V_{ion}, the voltage generated across the ion exchange membrane which is related to the difference in concentration of TMA^+ between the tip of the ISM and the backfill solution of this barrel (this voltage is a modified Nernst potential across the membrane). The second component is the LFP in the vicinity of the ISM tip. These two components sum to yield V_1. To compute the concentration of TMA registered at the tip of the ISM, the LFP must be subtracted from V_1 to obtain V_{ion}. To do this the LFP must be measured and subtracted. This is accomplished by using the second barrel of the ISM (reference barrel) to measure V_2, the LFP alone, with a conventional electrolyte-filled barrel. The potentials V_1 and V_2 pass through impedance-matching amplifiers (also known as headstages) each with 1× gain and then V_2 is subtracted from V_1 with a suitably configured summing amplifier. This provides the pure V_{ion} signal ($V_1 - V_2 = V_{ion}$). This must now be converted to a signal representing the concentration. To accomplish this, V_{ion} is fed into a computer (via an a/d converter) and the Nicolsky equation (the modified Nernst equation) along with suitable prior calibration data applied to finally yield C_{ion}, the concentration measured at the tip of the ISM. The LFP, V_2, is essentially the voltage detected on the second barrel of the ISM. With this background we can now provide several sets of evidence that the RVP signals are real.

1. Directionalities of the RVP events and the LFP excursions (Fig. 7B). Epileptiform voltage waveforms detected on the LFP traces (V_2) can be upwards or downwards or bidirectional while the concomitant RVP events (C_{ion}, shown as Δ [TMA^+]) were always unidirectional. Had the RVP events contained the LFP excursions, its directionality would mirror, at least partially, the directionality of the LFP excursions.

2. Amplitudes of RVP voltages and LFP excursions (Fig. 7C). As explained earlier, the RVP events are initially recorded as voltages ($V_1 - V_2 = V_{ion}$) at the same gain as the epileptiform activity on LFP traces (V_2). When we compare the amplitudes of RVP voltages ($V_1 - V_2$) with the amplitudes of LFP excursions (V_2), RVP voltages are larger, sometimes several-fold. Even if we assume that the RVP signal is picking up the same voltage recorded as LFPs, it is difficult to imagine that the signal would be magnified.

3. RVP events recorded with an anionic ECS molecular probe (Fig. 7D). Most experiments were performed using cation TMA^+ as an ECS probe. In a separate experiment, we verified that RVP can be measured with another ECS probe, anion alpha-naphthalene sulfonate (α-NS^-). When TMA^+ concentration increases, the voltage signal ($V_1 - V_2$) is upwards. We found that for RVP detected with TMA^+, voltage excursions were always upwards. When α-NS^- concentration increases, the voltage signal ($V_1 - V_2$) is downwards. We found that for RVP detected with α-NS^-, voltage excursions were always downwards. If the RVP voltages were artefacts related to the LFP excursions, we would not

consistently see opposite polarities for the voltages corresponding to the cationic probe TMA^+ and the voltages corresponding to the anionic probe α-NS^-.

4. Subtraction of LFP excursions from ion signal (Fig. 7E). The PTQ method utilizes a double-barrelled ISM to record the RVP events as changes in a concentration of extracellular molecular probe on the 'ion-selective barrel'; the LFPs are recorded on the 'reference barrel' (Fig. 7A). The voltage corresponding to the concentration of extracellular molecular probe is extracted at the dual-channel amplifier by subtracting the voltage on a reference barrel from the voltage on an ion barrel. To demonstrate that this differencing amplification feature is functional for short voltage excursions similar to the epileptiform waveforms on LFP trace, we performed a test experiment. We utilized an iontophoretic microelectrode (filled with 150 mM NaCl) to deliver a train of square current pulses in agarose and we detected the resulting voltages in the agarose with a TMA-ISM. First, we detected the pulses without engaging the subtraction feature on the amplifier. Under this scenario, voltage excursions were observed on the signals coming from both barrels (V_1, V_2; Fig. 7E left). Then, we repeated the experiment but this time the subtraction feature was switched on ($V_1 - V_2$). Under this scenario (which is used to record RVP and LFP events in brain tissue experiment), voltage excursions were observed on the signal coming from the reference barrel (V_2) but not on the signal coming from the ion barrel ($V_1 - V_2$) (Fig. 7E right). This experiment demonstrates that when the subtraction is engaged, the ion concentration signal is not contaminated by the LFP excursions.

References

Andrew RD & MacVicar BA (1994). Imaging cell volume changes and neuronal excitation in the hippocampal slice. Neuroscience 62, 371–383. [PubMed: 7830884]

Andrew RD, Labron MW, Boehnke SE, Carnduff L & Kirov SA (2007). Physiological evidence that pyramidal neurons lack functional water channels. Cereb Cortex 17, 787–802. [PubMed: 16723408]

Arranz AM, Perkins KL, Irie F, Lewis DP, Hrabe J, Xiao F, Itano N, Kimata K, Hrabetova S & Yamaguchi Y (2014). Hyaluronan deficiency due to Has3 knock-out causes altered neuronal activity and seizures via reduction in brain extracellular space. J Neurosci 34, 6164–6176. [PubMed: 24790187]

Binder DK, Yao X, Zador Z, Sick TJ, Verkman AS & Manley GT (2006). Increased seizure duration and slowed potassium kinetics in mice lacking aquaporin-4 water channels. Glia 53, 631–636. [PubMed: 16470808]

Colbourn R, Naik A & Hrabetova S (2019). ECS dynamism and its influence on neuronal excitability and seizures. Neurochem Res 44, 1020–1036. [PubMed: 30879174]

Dalic L & Cook MJ (2016). Managing drug-resistant epilepsy: challenges and solutions. Neuropsychiatr Dis Treat 12, 2605–2616. [PubMed: 27789949]

Deitmer JW & Szatkowski M (1990). Membrane potential dependence of intracellular pH regulation by identified glial cells in the leech central nervous system. J Physiol 421, 617–631. [PubMed: 2112195]

Dietzel I, Heinemann U, Hofmeier G & Lux HD (1980). Transient changes in the size of the extracellular space in the sensorimotor cortex of cats in relation to stimulus-induced changes in potassium concentration. Exp Brain Res 40, 432–439. [PubMed: 6254790]

Dietzel I, Heinemann U & Lux HD (1989). Relations between slow extracellular potential changes, glial potassium buffering, and electrolyte and cellular volume changes during neuronal hyperactivity in cat brain. Glia 2, 25–44. [PubMed: 2523337]

Dudek FE, Snow RW & Taylor CP (1986). Role of electrical interactions in synchronization of epileptiform bursts. Adv Neurol 44, 593–617. [PubMed: 3706022]

Glykys J, Duquette E, Rahmati N, Duquette K, & Staley KJ (2019). Mannitol decreases neocortical epileptiform activity during early brain development via cotransport of chloride and water. Neurobiol Dis 125, 163–175. [PubMed: 30711483]

Goldenberg MM (2010). Overview of drugs used for epilepsy and seizures: etiology, diagnosis, and treatment. P T 35, 392–415. [PubMed: 20689626]

Gonzalez-Sulser A, Wang J, Motamedi GK, Avoli M, Vicini S & Dzakpasu R (2011). The 4-aminopyridine in vitro epilepsy model analyzed with a perforated multi-electrode array. Neuropharmacology 60, 1142–1153. [PubMed: 20955719]

Haj-Yasein NN, Jensen V, Østby I, Omholt SW, Voipio J, Kaila K, Ottersen OP, Hvalby Ø, & Nagelhus EA (2012). Aquaporin-4 regulates extracellular space volume dynamics during high-frequency synaptic stimulation: a gene deletion study in mouse hippocampus. Glia 60, 867–874. [PubMed: 22419561]

Hansen AJ & Olsen CE (1980). Brain extracellular space during spreading depression and ischemia. Acta Physiol Scand 108, 355–365. [PubMed: 7415848]

Hentschke M, Wiemann M, Hentschke S, Kurth I, Hermans-Borgmeyer I, Seidenbecher T, Jentsch TJ, Gal A & Hübner CA (2006). Mice with a targeted disruption of the $Cl^-/HCO3^-$ exchanger AE3 display a reduced seizure threshold. Mol Cell Biol 26, 182–191. [PubMed: 16354689]

Hochman DW (2012). The extracellular space and epileptic activity in the adult brain: explaining the antiepileptic effects of furosemide and bumetanide. Epilepsia 53, 18–25.

Hrabe J, Hrabetová S & Segeth K (2004). A model of effective diffusion and tortuosity in the extracellular space of the brain. Biophys J 87, 1606–1617. [PubMed: 15345540]

Hrabětová S & Nicholson C (2007). Biophysical Properties of Brain Extracellular Space Explored with Ion-Selective Microelectrodes, Integrative Optical Imaging and Related Techniques. In Electrochemical Methods for Neuroscience, ed. Michael AC & Borland LM, Chapter 10, pp. 167–204.CRC Press/Taylor and Francis.

Huber VJ, Tsujita M & Nakada T (2009). Identification of aquaporin 4 inhibitors using in vitro and in silico methods. Bioorg Med Chem 17, 411–417. [PubMed: 18182301]

Jo S-M, Ryu HJ, Kim J-E, Yeo S-I, Kim M-J, Choi H-C, Song H-K & Kang T-C (2011). Up-regulation of endothelial endothelin-1 expression prior to vasogenic edema formation in the rat piriform cortex following status epilepticus. Neurosci Lett 501, 25–30. [PubMed: 21742016]

Kaur G, Hrabetova S, Guilfoyle DN, Nicholson C & Hrabe J (2008). Characterizing molecular probes for diffusion measurements in the brain. J Neurosci Methods 171, 218–225. [PubMed: 18466980]

Kilb W, Dierkes PW, Syková E, Vargová L & Luhmann HJ (2006). Hypoosmolar conditions reduce extracellular volume fraction and enhance epileptiform activity in the CA3 region of the immature rat hippocampus. J Neurosci Res 84, 119–129. [PubMed: 16634058]

Kumar V, Naik RS, Hillert M & Klein J (2006). Effects of chloride flux modulators in an in vitro model of brain edema formation. Brain Res 1122, 222–229. [PubMed: 17014830]

Larsen BR, Assentoft M, Cotrina ML, Hua SZ, Nedergaard M, Kaila K, Voipio J & MacAulay N (2014). Contributions of the Na^+/K^+-ATPase, NKCC1, and Kir4.1 to hippocampal K^+ clearance and volume responses. Glia 62, 608–622. [PubMed: 24482245]

Larsen BR & MacAulay N (2017). Activity-dependent astrocyte swelling is mediated by pH-regulating mechanisms. Glia 65, 1668–1681. [PubMed: 28744903]

Larsen BR, Stoica A & MacAulay N (2019). Developmental maturation of activity-induced K^+ and pH transients and the associated extracellular space dynamics in the rat hippocampus. J Physiol 597, 583–597. [PubMed: 30357826]

Lee AC, Wong RKS, Chuang S-C, Shin H-S & Bianchi R (2002). Role of synaptic metabotropic glutamate receptors in epileptiform discharges in hippocampal slices. J Neurophysiol 88, 1625–1633. [PubMed: 12364493]

Lee DJ, Amini M, Hamamura MJ, Hsu MS, Seldin MM, Nalcioglu O & Binder DK (2012). Aquaporin-4-dependent edema clearance following status epilepticus. Epilepsy Res 98, 264–268. [PubMed: 21996149]

Liu R, Wang J, Liang S, Zhang G, & Yang X (2020). Role of NKCC1 and KCC2 in epilepsy: from expression to function. Front Neurol 10, 1407. [PubMed: 32010056]

Loucif KC, Wilson CL, Baig R, Lacey MG & Stanford IM (2005). Functional interconnectivity between the globus pallidus and the subthalamic nucleus in the mouse brain slice. J Physiol 567, 977–987. [PubMed: 16037086]

Lux HD, Heinemann U & Dietzel I (1986). Ionic changes and alterations in the size of the extracellular space during epileptic activity. Adv Neurol 44, 619–639. [PubMed: 3518349]

MacAulay N (2020). Molecular mechanisms of K^+ clearance and extracellular space shrinkage—glia cells as the stars. Glia 68, 2192–2211. [PubMed: 32181522]

Murphy TR, Binder DK & Fiacco TA (2017a). Turning down the volume: astrocyte volume change in the generation and termination of epileptic seizures. Neurobiol Dis 104, 24–32. [PubMed: 28438505]

Murphy TR, Davila D, Cuvelier N, Young LR, Lauderdale K, Binder DK & Fiacco TA (2017b). Hippocampal and cortical pyramidal neurons swell in parallel with astrocytes during acute hypoosmolar stress. Front Cell Neurosci 11, 275. [PubMed: 28979186]

N'Gouemo P (2011). Targeting BK (big potassium) channels in epilepsy. Expert Opin Ther Targets 15, 1283–1295. [PubMed: 21923633]

Nicholson C & Phillips JM (1981). Ion Diffusion Modified by Tortuosity and Volume Fraction in the Extracellular Microenvironment of the Rat Cerebellum. J Physiol 321, 225–257. [PubMed: 7338810]

Nwaobi SE, Cuddapah VA, Patterson KC, Randolph AC, Olsen ML (2016). The role of glial specific Kir4.1 in normal and pathological states of the CNS. Acta Neuropathol 132, 1–21. [PubMed: 26961251]

Odackal J, Colbourn R, Odackal NJ, Tao L, Nicholson C & Hrabetova S (2017). Real-time iontophoresis with tetramethylammonium to quantify volume fraction and tortuosity of brain extracellular space. J Vis Exp 125, e55755.

Ohno Y, Tokudome K, Kunisawa N, Iha HA, Kinboshi M, Mukai T, Serikawa T & Shimizu S (2015). Role of Astroglial Kir4.1 channels in the pathogenesis and treatments of epilepsy. Ther Targets Neurol Dis 2, e476.

Olsson T, Broberg M, Pope KJ, Wallace A, Mackenzie L, Blomstrand F, Nilsson M & Willoughby JO (2006). Cell Swelling, Seizures and Spreading Depression: An Impedance Study. Neuroscience 140, 505–515. [PubMed: 16580141]

Onodera M, Meyer J, Furukawa K, Hiraoka Y, Aida T, Tanaka K, Tanaka KF, Rose CR & Matsui K (2021). Exacerbation of epilepsy by astrocyte alkalization and gap junction uncoupling. J Neurosci 41, 2106–2118. [PubMed: 33478985]

Parker MD (2018). Mouse models of *SLC4*-linked disorders of HCO3−-transporter dysfunction. Am J Physiol Cell Physiol 314, C569–C588. [PubMed: 29384695]

Phillips JM & Nicholson C (1979). Anion permeability in spreading depression investigated with ion-sensitive microelectrodes. Brain Res 173, 567–571. [PubMed: 487110]

Ringel F, Chang RC, Staub F, Baethmann A & Plesnila N (2001). Contribution of anion transporters to the acidosis-induced swelling and intracellular acidification of glial cells. J Neurochem 75, 125–132.

Rungta RL, Choi HB, Tyson JR, Malik A, Dissing-Olesen L, Lin PJC, Cain SM, Cullis PR, Snutch TP & MacVicar BA (2015). The cellular mechanisms of neuronal swelling underlying cytotoxic edema. Cell 161, 610–621. [PubMed: 25910210]

Salah A & Perkins KL (2011). Persistent ictal-like activity in rat entorhinal/perirhinal cortex following washout of 4-aminopyridine. Epilepsy Res 94, 163–176. [PubMed: 21353480]

Sherpa AD, van de Nes P, Xiao F, Weedon J & Hrabetova S (2014). Gliotoxin-induced swelling of astrocytes hinders diffusion in brain extracellular space via formation of dead-space microdomains. Glia 62, 1053–1065. [PubMed: 24687699]

Sinning A & Hübner CA (2013). Minireview: pH and synaptic transmission. FEBS Lett 587, 1923–1928. [PubMed: 23669358]

Sivakumaran S, Cardarelli RA, Maguire J, Kelley MR, Silayeva L, Morrow DH, Mukherjee J, Moore YE, Mather RJ, Duggan ME, Brandon NJ, Dunlop J, Zicha S, Moss SJ & Deeb TZ (2015). Selective inhibition of KCC2 leads to hyperexcitability and epileptiform discharges in hippocampal slices and in vivo. J Neurosci 35, 8291–8296. [PubMed: 26019342]

Slais K, Vorisek I, Zoremba N, Homola A, Dmytrenko L & Sykova E (2008). Brain metabolism and diffusion in the rat cerebral cortex during pilocarpine-induced status epilepticus. Exp Neurol 209, 145–154. [PubMed: 17961555]

Steffensen AB, Sword J, Croom D, Kirov SA & MacAulay N (2015). Chloride cotransporters as a molecular mechanism underlying spreading depolarization-induced dendritic beading. J Neurosci 35, 12172–12187. [PubMed: 26338328]

Sword J, Croom D, Wang PL, Thompson RJ & Kirov SA (2017). Neuronal pannexin-1 channels are not molecular routes of water influx during spreading depolarization-induced dendritic beading. J Cereb Blood Flow Metab 37, 1626–1633. [PubMed: 26994044]

Syková E, Vorísek I, Antonova T, Mazel T, Meyer-Luehmann M, Jucker M, Hájek M, Ort M & Bures J (2005). Changes in extracellular space size and geometry in app23 transgenic mice: a model of Alzheimer's disease. Proc Natl Acad Sci U S A 102, 479–484. [PubMed: 15630088]

Syková E & Nicholson C (2008). Diffusion in brain extracellular space. Physiol Rev 88, 1277–1340. [PubMed: 18923183]

Theparambil SM, Ruminot I, Schneider H-P, Shull GE & Deitmer JW (2014). The electrogenic sodium bicarbonate cotransporter NBCe1 is a high-affinity bicarbonate carrier in cortical astrocytes. J Neurosci 34, 1148–1157. [PubMed: 24453308]

Theparambil SM, Naoshin Z, Thyssen A & Deitmer JW (2015). Reversed electrogenic sodium bicarbonate cotransporter 1 is the major acid loader during recovery from cytosolic alkalosis in mouse cortical astrocytes. J Physiol 593, 3533–3547. [PubMed: 25990710]

Toft-Bertelsen TL, Larsen BR, Christensen SK, Khandelia H, Waagepetersen HS & MacAulay N (2020). Clearance of activity-evoked K^+ transients and associated glia cell swelling occur independently of AQP4: A study with an isoform-selective AQP4 inhibitor. Glia 69, 28–41. [PubMed: 32506554]

Tønnesen J, Inavalli VVGK & Nägerl UV (2018). Super-resolution imaging of the extracellular space in living brain tissue. Cell 172, 1108–1121. [PubMed: 29474910]

Traynelis SF & Dingledine R (1989). Role of extracellular space in hyperosmotic suppression of potassium-induced electrographic seizures. J Neurophysiol 61, 927–938. [PubMed: 2723735]

Uwera J, Nedergaard S & Andreasen M (2015). A novel mechanism for the anticonvulsant effect of furosemide in rat hippocampus in vitro. Brain Res 1625, 1–8. [PubMed: 26301821]

Velíšek L, Dreier JP, Stanton PK, Heinemann U & Moshé SL (1994). Lowering of extracellular pH Suppresses low-Mg^{2+}-induces seizures in combined entorhinal cortex-hippocampal slices. Exp Brain Res 101, 44–52. [PubMed: 7843301]

Walch E, Murphy TR, Cuvelier N, Aldoghmi M, Morozova C, Donohue J, Young G, Samant A, Garcia S, Alvarez C, Bilas A, Davila D, Binder DK & Fiacco TA (2020). Astrocyte-selective volume increase in elevated extracellular potassium conditions is mediated by the Na^+/K^+ ATPase and occurs independently of aquaporin 4. ASN Neuro 12, 175909142096715.

Weiss SA & Faber DS (2010). Field effects in the CNS play functional roles. Front Neural Circuits 4, 15. [PubMed: 20508749]

Wu Z, Huo Q, Ren L, Dong F, Feng M, Wang Y, Bai Y, Lüscher B, Li S-T, Wang G-L, Long C, Wang Y, Wu G & Chen G (2019). Gluconate suppresses seizure activity in developing brains by inhibiting CLC-3 chloride channels. Mol Brain 12, 50. [PubMed: 31088565]

Xie L, Kang H, Xu Q, Chen MJ, Liao Y, Thiyagarajan M, O'Donnell J, Christensen DJ, Nicholson C, Iliff JJ, Takano T, Deane R & Nedergaard M (2013). Sleep Drives metabolite clearance from the adult brain. Science 342, 373–377. [PubMed: 24136970]

Xiong W, Ping X, Ripsch MS, Chavez GSC, Hannon HE, Jiang K, Bao C, Jadhav V, Chen L, Chai Z, Ma C, Wu H, Feng J, Blesch A, White FA & Jin X (2017). Enhancing excitatory activity of

somatosensory cortex alleviates neuropathic pain through regulating homeostatic plasticity. Sci Rep 7, 12743. [PubMed: 28986567]

Yang T, Lin Z, Xie L, Wang Y & Pan S (2017). 4,4′-Diisothiocyanatostilbene-2,2′-disulfonic acid attenuates spontaneous recurrent seizures and vasogenic edema following lithium-pilocarpine induced status epilepticus. Neurosci Lett 653, 51–57. [PubMed: 28501694]

Zhou Y, Zeng X-H & Lingle CJ (2012). Barium ions selectively activate BK channels via the Ca^{2+}-bowl site. Proc Natl Acad Sci U S A 109, 11413–11418. [PubMed: 22733762]

Key points

- Extracellular space (ECS) rapid volume pulsation (RVP) accompanying epileptiform activity is described for the first time.
- Such RVP occurs robustly in several *in vitro* and *in vivo* mouse models of epileptiform activity.
- In the *in vitro* 4-aminopyridine model of epileptiform activity, RVP depends on the activity of the electrogenic Na^+/HCO_3^- cotransporter (NBCe1).
- NBCe1 pharmacological inhibition suppresses RVP and epileptiform activity.
- Inhibition of changes in ECS volume may be a useful target in epilepsy patients who are resistant to current treatments.

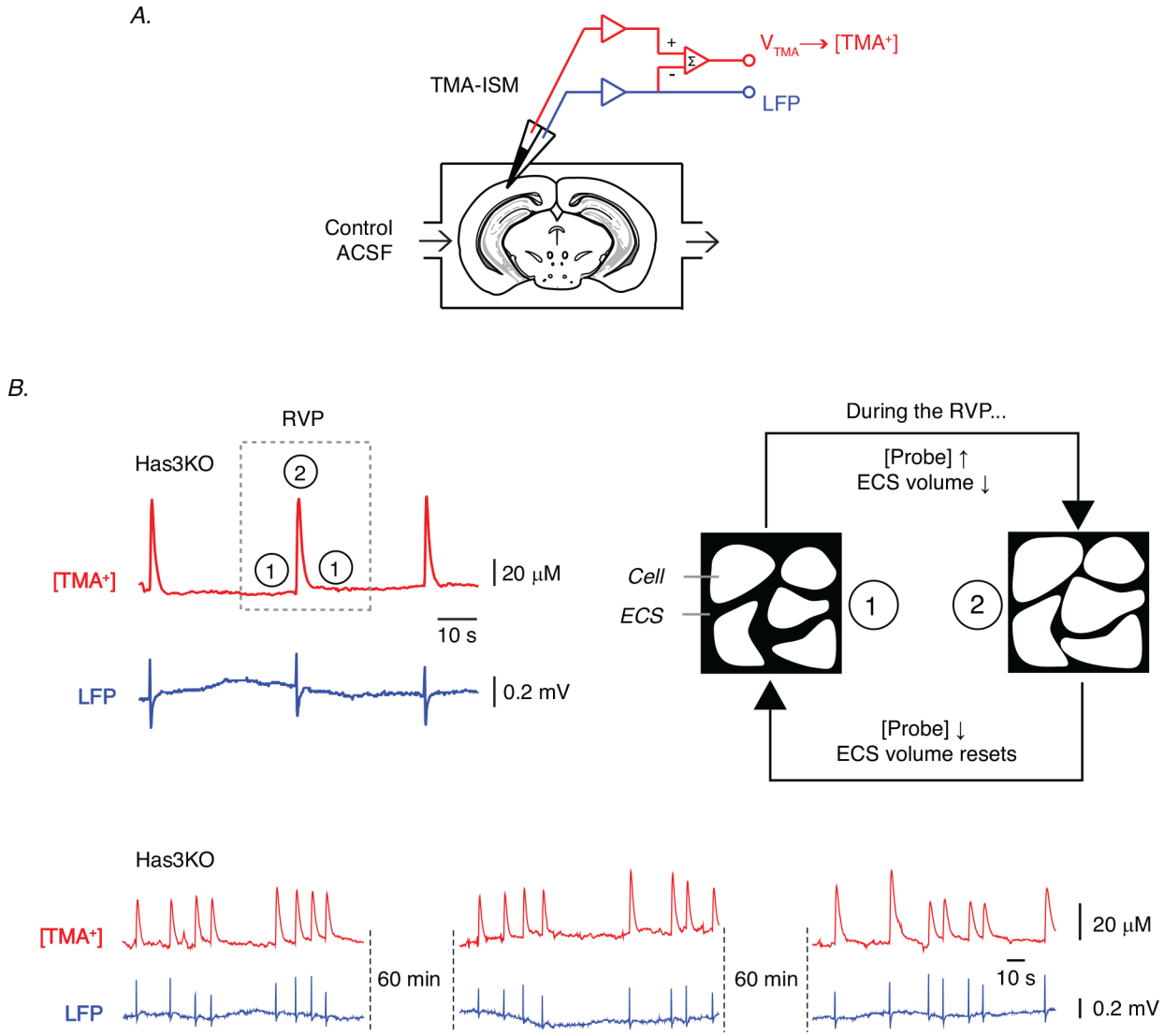

Figure 1. Rapid volume pulsation (RVP) events revealed with the probe transients quantification (PTQ) technique in the Has3KO model of spontaneous epileptiform activity

A, a schematic of the setup for the PTQ technique *in vitro*. Brain slices are incubated in control ACSF (containing 0.5 mM TMA-Cl) during the experiment. The ion-selective barrel (blackened tip) records the concentration of the molecular probe of the ECS (i.e. TMA^+) and the reference barrel (clear tip) records LFP events. *B*, representative records taken in the hippocampal slice from a knock-out mouse for hyaluronan synthase 3 (Has3KO; top left). LFP recording (blue traces) revealed waveforms that indicate spontaneous epileptiform activity is occurring. Fluctuations in the TMA^+ signal (red traces) indicate repeated RVP occurring concurrently with the events of epileptiform activity. A cartoon depicts the interpretation of TMA^+ signal (top right). RVP events and LFP events persisted for as long as we recorded, as shown in a representative recording taken over a period of 2 h (bottom). [Colour figure can be viewed at wileyonlinelibrary.com]

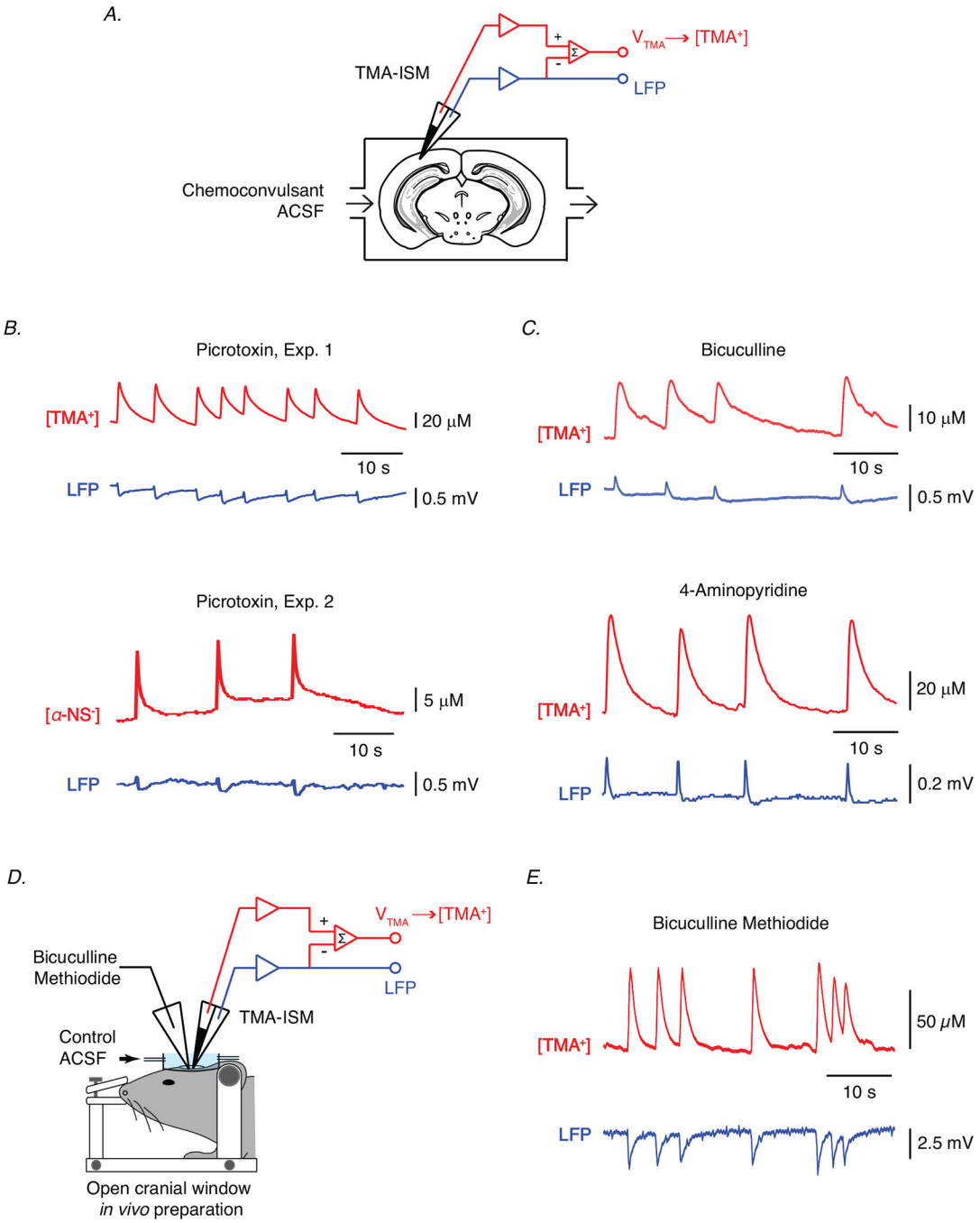

Figure 2. RVP events revealed with the PTQ technique across a range of mouse models of chemoconvulsant-induced epileptiform activity *in vitro* and *in vivo*

A, the *in vitro* setup for the PTQ technique. Chemoconvulsant ACSF (containing 0.5 mM TMA-Cl) is bath-applied to the brain slice to induce epileptiform activity. *B*, sample traces of RVP events and epileptiform activity induced in the visual cortex by picrotoxin (50 μM). RVP events were recorded with two different molecular probes of the ECS: TMA^+ (top) and anion alpha-naphthalene sulfonate (α-NS^-, bottom). *C*, RVP events induced in two additional *in vitro* models of epileptiform activity: bicuculline (50 μM, top) and 4-aminopyridine (100 μM, bottom). Both recordings were taken in the visual cortex. *D*, a

schematic showing the setup of the *in vivo* PTQ experiment. Control ACSF (containing 1 mM TMA-Cl) was flowing over the brain surface. Chemoconvulsant bicuculline methiodide (20 mM) was released from a pressure injection pipette placed near the ISM. *E*, a representative record of the signals obtained by the ISM during bicuculline methiodide-induced epileptiform activity *in vivo*. Similar to the *in vitro* experiment, there are transient changes in the TMA^+ signal (red trace) that signify RVP events occurring concurrently with the epileptiform waveforms on LFP trace (blue trace). [Colour figure can be viewed at wileyonlinelibrary.com]

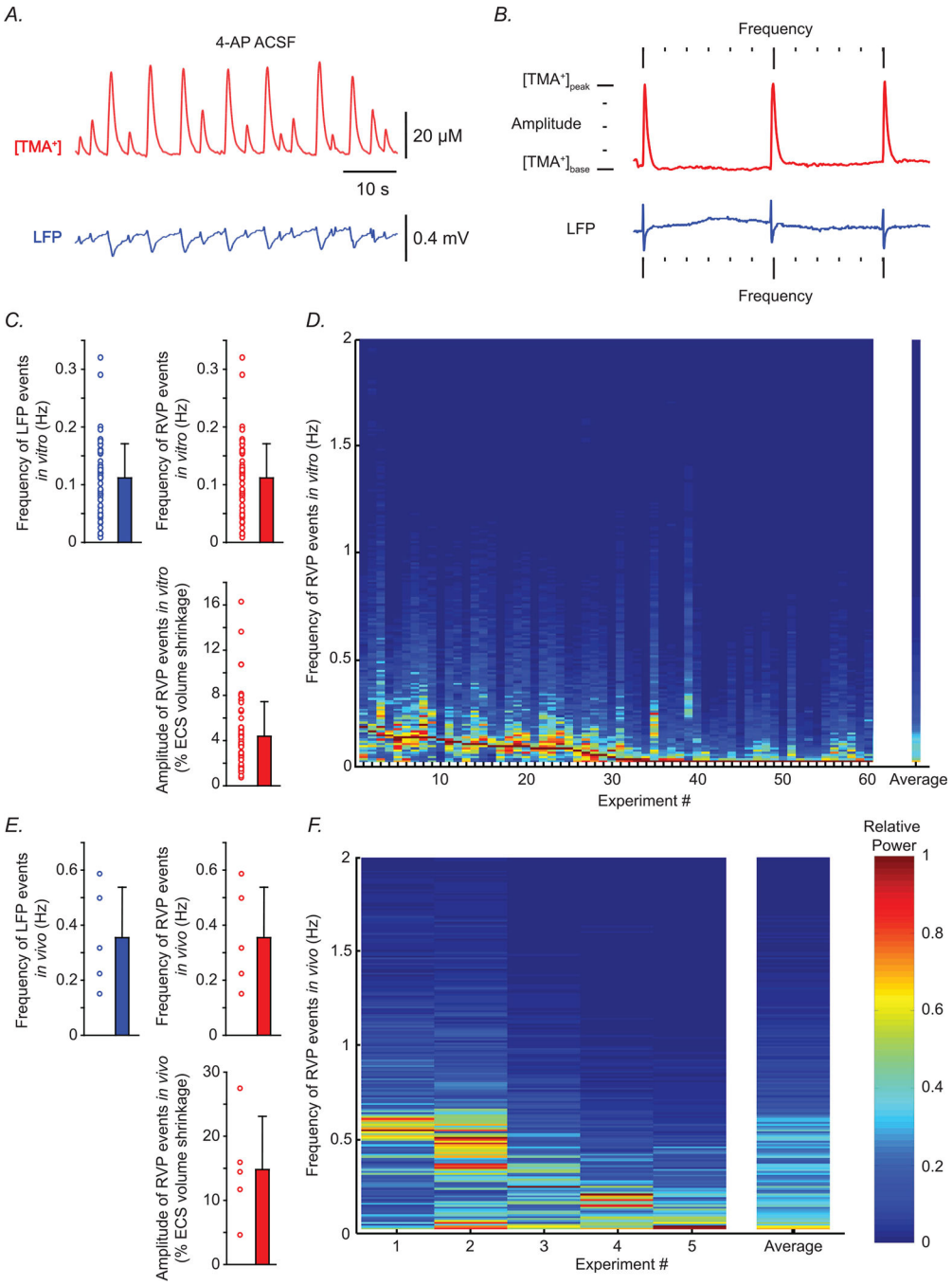

Figure 3. The quantification of RVP across the 4-AP *in vitro* model and the bicuculline methiodide *in vivo* model

A, a representative PTQ record taken during 4-AP-induced epileptiform activity *in vitro*. *B*, a schematic showing the parameters used to characterize the LFP and RVP events. *C*, graphs summarizing parameters extracted from 10 min segments of TMA^+ and LFP signals across all *in vitro* experiments ($n = 60$ slices, $N = 48$ animals). The mean frequency of epileptiform events on the LFP trace was 0.11 ± 0.06 Hz. The mean frequency of RVP matched that of LFP events. The mean amplitude of the RVP represented 4.4% ± 3.1% shrinkage of ECS volume. *D*, colour map summarizing a Fourier analysis performed on the 10 min segments

of TMA^+ signals across all *in vitro* experiments. An average column, which simply takes the mean of the normalized power spectra across all experiments, is shown on the right, and indicates that the TMA^+ signals are predominantly low frequency. *E*, graphs summarizing parameters extracted from 10 min segments of TMA^+ and LFP signals across all *in vivo* experiments ($n = 5$ slices, $N = 5$ animals). The mean frequency of epileptiform events on the LFP trace was 0.35 ± 0.18 Hz. The mean frequency of RVP matched that of LFP events. The mean amplitude of RVP represented 14.8% ± 8.3% shrinkage of ECS volume. *F*, colour map summarizing a Fourier analysis performed on the 10 min segments of TMA^+ signal across all *in vivo* experiments. [Colour figure can be viewed at wileyonlinelibrary.com]

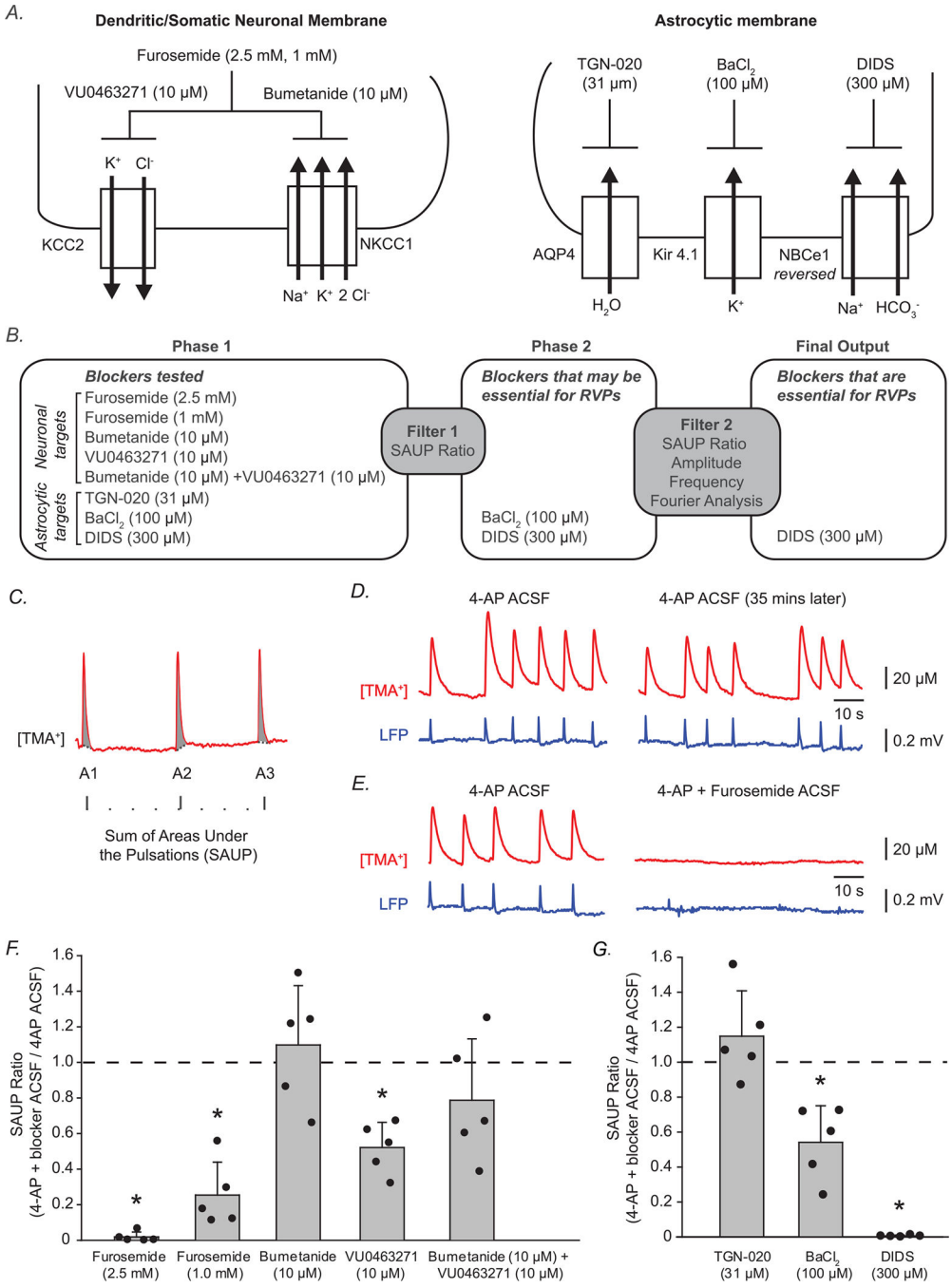

Figure 4. Outline of two-phase search for mechanism (*A*–*B*) and effects of the phase 1 blockers on RVP in the 4-AP *in vitro* model of epileptiform activity (*C*–*G*)

A, cartoon depicting the transporters and channels studied and the drugs used to block them. *B*, a flowchart of the two-phase study. In phase 1, PTQ was conducted under two conditions: one where the slice is superfused with 4-AP ACSF, and a subsequent one during which the slice is superfused with a blocker ACSF (see Table 1). SAUP analysis is used as the first filter to eliminate blockers that are unlikely to be targeting a channel/transporter necessary for RVP generation. Phase 2 involved repeating the PTQ experiments with selected candidate blockers, but analysing additional metrics to determine the blockers'

effect on RVP and epileptiform activity. Passing the second filter would indicate that a blocker diminished both RVP and epileptiform activity. *C*, diagram depicting SAUP analysis of RVP (eqns 2 and 3). *D*, control traces showing RVP and epileptiform activity in a slice superfused with 4-AP ACSF. The time period of the trace on the left matches the typical 4-AP recording period (i.e. 35 min after 4-AP wash-on), while the trace on the right matches the time period of the typical blocker recording period (i.e. 70 min after 4-AP wash-on). *E*, representative records taken from the 4-AP ACSF period (left) and 4-AP + furosemide (2.5 mM) ACSF period (right) of an experiment. During 4-AP + furosemide ACSF application, RVP and epileptiform activity were both eliminated. *F*, summary bar graph of the experiments investigating the NKCC1/KCC2 transporter blockades ($n = 5$ slices from $N = 5$ animals per group). The results showed a very large drop in the magnitude of RVP during 4-AP + furosemide ACSF application at two different concentrations (furosemide 2.5 mM: 0.0186 ± 0.0277, $P < 0.0001$, paired *t* test; furosemide 1 mM: 0.254 ± 0.185, $P = 0.0008$, paired *t* test), but these were not replicated using other specific blockers (bumetanide: 1.098 ± 0.333, $P = 0.547$, paired *t* test; VU0463271: 0.521 ± 0.141, $P = 0.002$, paired *t* test; bumetanide + VU0463271: 0.787 ± 0.345 $P = 0.240$, paired *t* test). *G*, summary bar graph of the experiments investigating the blockages of AQP4, Kir 4.1 and NBCe1 ($n = 5$ slices from $N = 5$ animals per group). While TGN-020 (31 μM; 1.149 ± 0.260, $P = 0.269$, paired *t* test) showed no effect, $BaCl_2$ (100 μM; 0.541 ± 0.209, $P = 0.008$, paired *t* test) and DIDS (300 μM; 0.0060 ± 0.0046, $P < 0.0001$, paired *t* test) both showed large effects on the magnitude of RVP. [Colour figure can be viewed at wileyonlinelibrary.com]

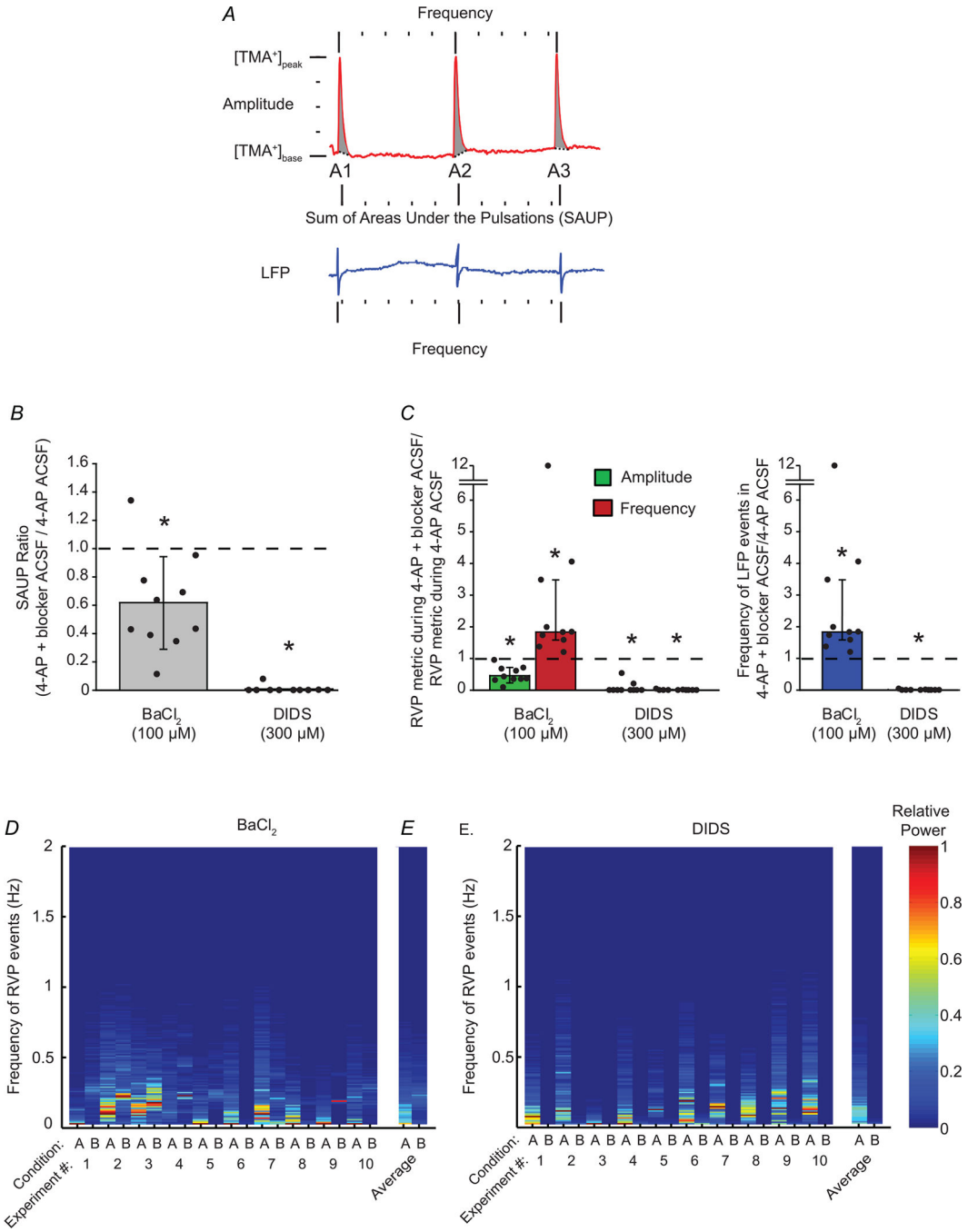

Figure 5. Effects of the phase 2 blockers on RVP and epileptiform activity in the 4-AP *in vitro* model

A, schematic showing the metrics analysed on the RVP and LFP events. *B*, summary bar graph of the SAUP analysis for $BaCl_2$ and DIDS ($n = 10$ slices from $N = 10$ animals per group). Both blockers caused statistically significant drops in SAUP ($BaCl_2$: 0.610 ± 0.352, mean ± SD, $P = 0.007$, paired t test; DIDS: median was 0.000, 25% quartile was 0.000, 75% quartile was 0.000, $P = 0.002$, Wilcoxon's signed rank test). DIDS had a much greater effect compared with $BaCl_2$. *C*, (left) summary bar graph comparing the amplitude and frequency of RVP events between the blocker and pre-blocker condition of DIDS and

$BaCl_2$ experiments. Amplitude of RVP dropped in $BaCl_2$ (0.483 ± 0.249, mean ± SD, $P = 0.0001$, paired t test) and DIDS (median was 0.000, 25% quartile was 0.000, 75% quartile was 0.000, $P = 0.002$, Wilcoxon's signed rank test). However, the frequency of RVP increased in $BaCl_2$ (median was 1.83, 25% quartile was 1.58, 75% quartile was 3.48, $P = 0.002$, Wilcoxon's signed rank test) and decreased in DIDS (median was 0.000, 25% quartile was 0.000, 75% quartile was 0.000, $P = 0.002$, Wilcoxon's signed rank test). (Right) The frequency of epileptiform activity in the blocker period followed the same pattern as the frequency of RVP events: the frequency of epileptiform activity increased during $BaCl_2$ application (median was 1.83, 25% quartile was 1.58, 75% quartile was 3.48, $P = 0.002$, Wilcoxon's signed rank test), and epileptiform activity was almost complete elimination during DIDS application (median was 0.000, 25% quartile was 0.000, 75% quartile was 0.000, $P = 0.002$, Wilcoxon's signed rank test). *D*, colour map summarizing the power spectra for $BaCl_2$ experiments. Per experiment, two power spectra were obtained during two conditions: A (4-AP ACSF application) and B (Blocker ACSF application). This map shows that during many of the experiments, all frequencies dropped in power, and the highest-powered frequency tended to become more frequent. This is corroborated in the 'average' columns, which show the highest power in the A condition at the lowest frequency, but B's largest relative power occurs at a higher frequency. *E*, colour map summarizing the power spectra for DIDS experiments. Here, all experiments show high power in the A conditions, with almost complete elimination of all signals in the B conditions. This is evident in the 'average' columns as well. [Colour figure can be viewed at wileyonlinelibrary.com]

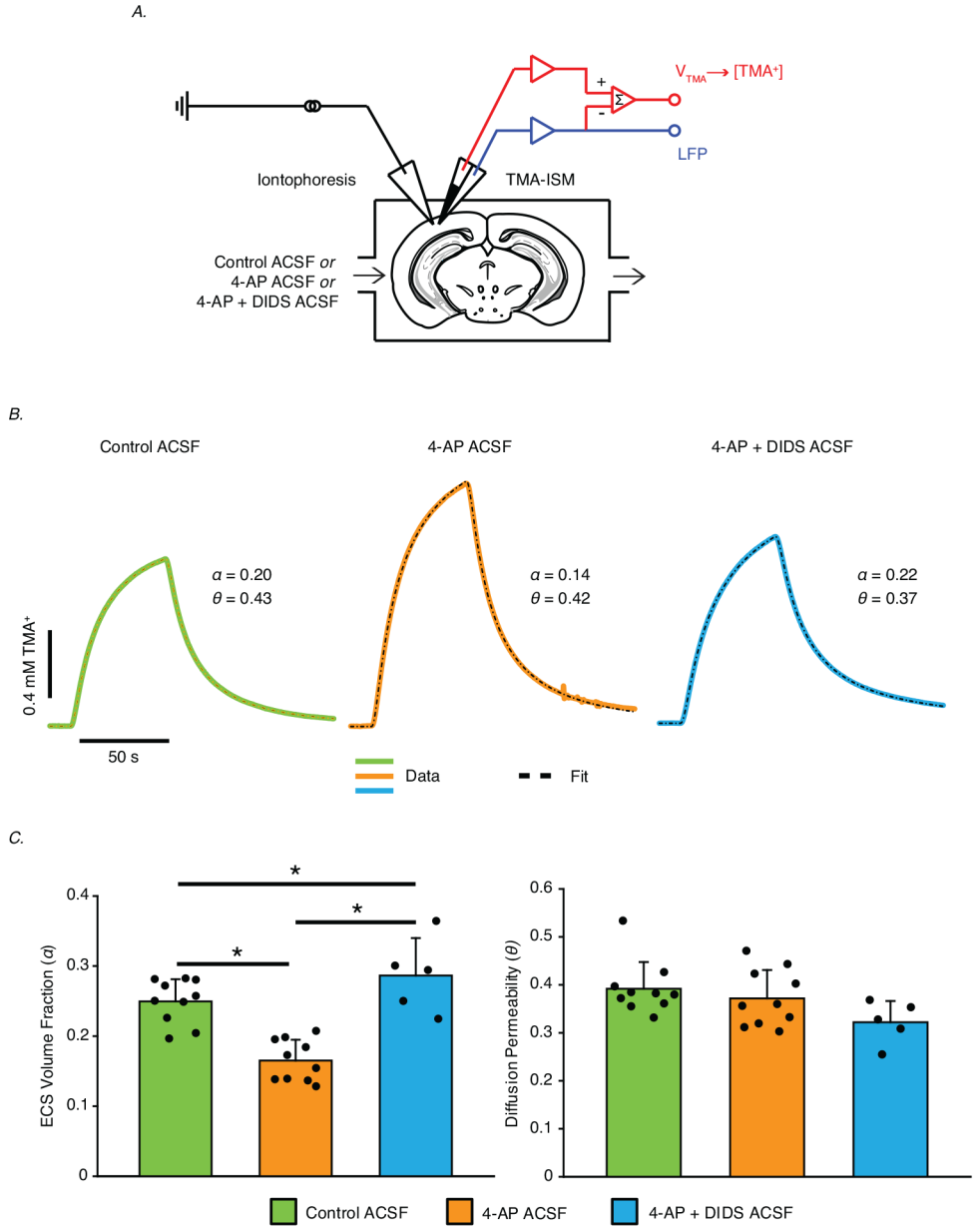

Figure 6. RTI experiments determine SES during epileptiform activity in 4-AP *in vitro* model and after application of DIDS

A, schematic depicting the setup of the RTI experiment. The setup is similar to PTQ and employs the same ISM-amplifier arrangement. In addition, an iontophoretic microelectrode is placed at a fixed distance from the TMA-ISM. *B*, RTI measurements were taken during three phases of this experiment. First, during control ACSF application (T = 34.1°C, r = 120 μm, n_t = 0.329, κ = 0.0077 s^{-1}). Second, during 4-AP (100 μM) ACSF application (T = 34.2°C, r = 120 μm, n_t = 0.329, κ = 0.0048 s^{-1}). Third, after 4-AP + DIDS (300 μM) ACSF application (T = 33.8°C, r = 120 μm, n_t = 0.329, κ = 0.0015 s^{-1}). *C*, summary bar graphs of ECS volume fraction α and diffusion permeability θ across the three conditions. (Left graph) ECS volume fraction significantly dropped between control ACSF (α = 0.25

± 0.03) and 4-AP ACSF (α = 0.16 ± 0.03) applications (n = 10 slices, N = 10 animals, P = 0.000008, repeated measures one-way ANOVA with Bonferroni *post hoc*), then rose between 4-AP ACSF and 4-AP + DIDS ACSF (α = 0.29 ± 0.05) applications (n = 10 slices, N = 10 animals for 4-AP condition, n = 5 slices, N = 5 animals for 4-AP + DIDS condition, P = 0.000002, repeated measures one-way ANOVA with Bonferroni *post hoc*). The 4-AP + DIDS condition had a significantly higher ECS volume fraction than the control condition (P = 0.034, repeated measures one-way ANOVA with Bonferroni *post hoc*). (Right graph) Diffusion permeability θ was unaffected across all three conditions (control: 0.392 ± 0.056, 4-AP: 0.372 ± 0.059, 4-AP + DIDS: 0.322 ± 0.044; P = 0.06, repeated measures one-way ANOVA). [Colour figure can be viewed at wileyonlinelibrary.com]

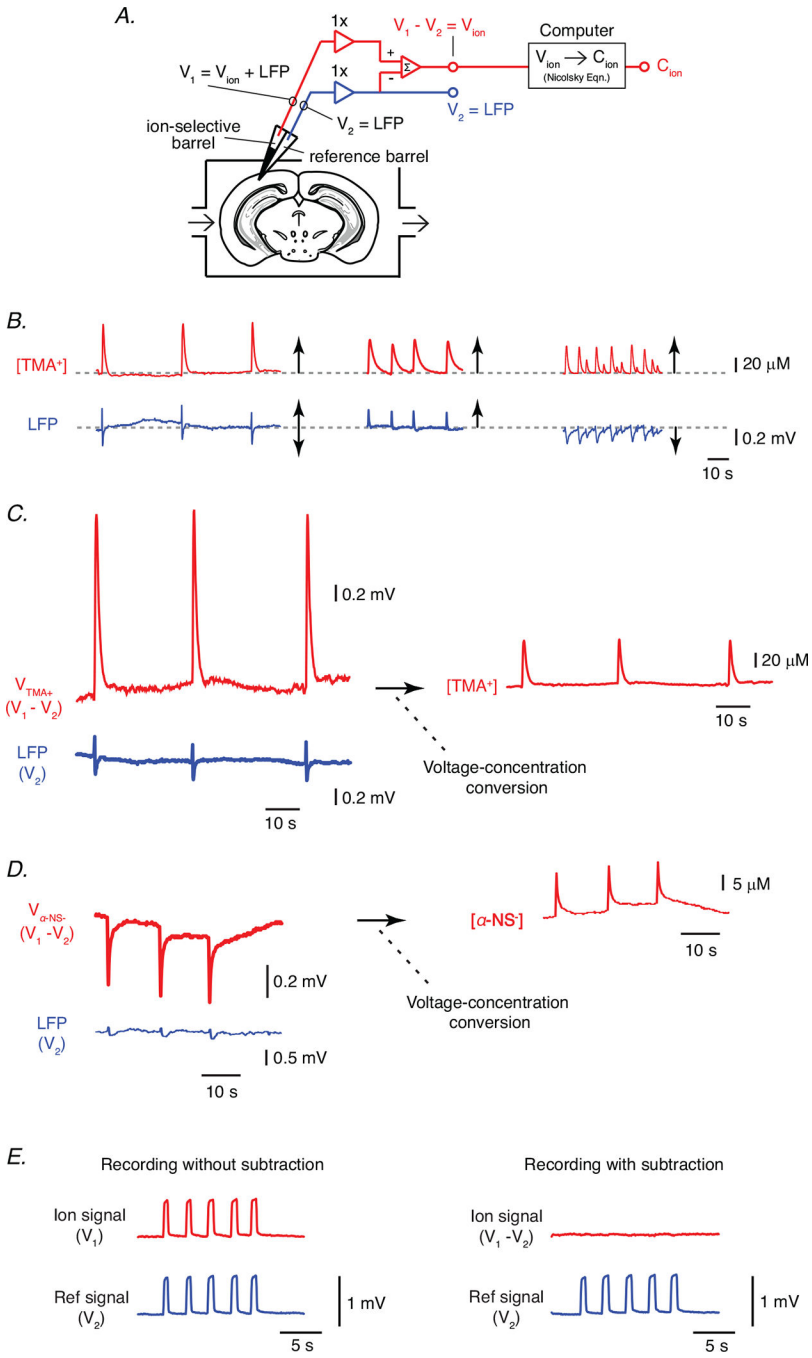

Figure 7. The RVP phenomenon is real

See Appendix for details. [Colour figure can be viewed at wileyonlinelibrary.com]

Table 1.

Reference table for ACSF compositions

ACSF category	ACSF label	Composition	Purpose
Control	Control	NaCl 124, KCl 5, $NaHCO_3$ 26, NaH_2PO_4 1.25, D-glucose 10, $MgCl_2$ 1.3, $CaCl_2$ 1.5, 0.5 TMA-Cl (1.0 TMA-Cl for *in vivo*) or 0.5 α-NS^-	To maintain tissue integrity and provide baseline TMA-Cl concentration
Base for chemo-convulsant	Low divalent	NaCl 124, KCl 5, $NaHCO_3$ 26, NaH_2PO_4 1.25, D-glucose 10, $MgCl_2$ 0.6, $CaCl_2$ 1.2, 0.5 TMA-Cl or 0.5 α-NS^-	To assist in generating epileptiform activity in all models (Salah & Perkins, 2011)
	4-aminopyridine (4-AP)	Low divalent + 100 μM 4-AP (catalogue #275875, Sigma-Aldrich)	To generate epileptiform activity by blocking voltage-gated K^+ currents (Salah & Perkins, 2011)
Chemoconvulsant	Picrotoxin	Low divalent + 50 μM picrotoxin (catalogue #P1675, Sigma-Aldrich)	To generate epileptiform activity by blocking $GABA_A$ receptors (Loucif *et al.* 2005)
	Bicuculline	Low divalent + 50 μM bicuculline (catalogue #14340, Sigma-Aldrich)	To generate epileptiform activity by blocking $GABA_A$ receptors (Lee *et al.* 2002)
Blocker	4-AP + furosemide	4-AP ACSF + 2.5 mM or 1 mM furosemide (catalogue #F4381, Sigma-Aldrich)	To block NKCC1 + KCC2 transporters (Hochman, 2012)
	4-AP + bumetanide	4-AP ACSF + 10 μM bumetanide (catalogue #B3023, Sigma-Aldrich)	To block NKCC1 transporters (Hochman, 2012)
	4-AP + VU0463471	4-AP ACSF + 10 μM VU0463271 (catalogue #SML0136, Sigma-Aldrich)	To block KCC2 transporters (Sivakumaran *et al.* 2015)
	4-AP + $BaCl_2$	4-AP ACSF + 100 μM $BaCl_2$ (catalogue #202738, Sigma-Aldrich)	To block Kir4.1 channels (Larsen & MacAulay, 2014)
	4-AP + TGN-020	4-AP ACSF + 31 μM TGN-020 (catalogue #SML0136, Sigma-Aldrich)	To block AQP4 channels (Huber *et al.* 2009)
	4-AP + DIDS	4-AP ACSF + 300 μM DIDS (catalogue #4523, Tocris Bioscience)	To block NBCe1 transporters (Larsen & MacAulay, 2017)

All concentrations are in mM unless otherwise specified.